Tailored Polarizing Hybrid Solids with Nitroxide Radicals Localized in Mesostructured Silica Walls.

Daniel L. Silverio, Henri A. van Kalkeren, Ta-Chung Ong, Mathieu Baudin, Maxim Yulikov, Laurent Veyre, Pierrick Berruyer, Sachin Chaudhari, David Gajan, David Baudouin, Matthieu Cavaillès, Basile Vuichoud, Aurélien Bornet, Gunnar Jeschke, Geoffrey Bodenhausen, Anne Lesage, Lyndon Emsley, Sami Jannin, Chloé Thieuleux,* and Christophe Copéret*

Abstract: Hyperpolarization by dynamic nuclear polarization relies on the microwave irradiation of paramagnetic radicals dispersed in molecular glasses to enhance the nuclear magnetic resonance (NMR) signals of target molecules. However, magnetic or chemical interactions between the radicals and the target molecules can lead to attenuation of the NMR signal through paramagnetic quenching and/or radical decomposition. Here we describe polarizing materials incorporating nitroxide radicals *within the walls* of the solids to minimize interactions between the radicals and the solute. These materials can hyperpolarize pure pyruvic acid, a particularly important substrate of clinical interest, while nitroxide radicals cannot be used, even when incorporated in the pores of silica, because of reactions between pyruvic acid and the radicals. The properties of these materials can be engineered by tuning the composition of the wall by introducing organic functionalities.

Introduction

Dynamic nuclear polarization (DNP) provides a way to dramatically enhance NMR signals, and as a result has opened new frontiers in the characterization of a broad range of molecules (e.g., biomolecules, metabolites, surface species, complex materials, etc.).[1] In a DNP experiment, the Boltzmann polarization of electron spins of unpaired electrons (e.g., stable radicals such as nitroxides or trityls) is partially transferred to the nuclear spins of the target molecules.[2] This polarization transfer leads to NMR signal enhancement (ε) and thereby a reduction of the acquisition time. Proton polarization can propagate throughout the entire frozen sample via spin diffusion, and cross polarization (CP) from protons can be used to obtain sensitivity-enhanced NMR signals of heteronuclei (e.g., ^{13}C, ^{29}Si, etc.).

DNP is increasingly used to enhance the sensitivity of solid-state NMR spectra at cryogenic temperatures (100 K) under magic angle spinning (MAS-DNP) conditions,[2b] or for hyperpolarizing metabolites at 1.2 K that are rapidly dissolved and transferred to solution NMR spectrometers or MRI scanners (dissolution-DNP).[3] Biologically relevant hyperpolarized analytes or metabolites can be administered to cell cultures or living animals to reveal metabolic activity allowing, [3b, 3d, 4] *inter alia*, a reliable diagnosis of prostate cancer.[5] However, this kind of DNP experiment suffers from several limitations. Notably, the radicals must be soluble in a solvent that forms a glass at cryogenic temperature to ensure their homogeneous distribution. The radicals should not be in close contact with the analyte, as this can lead to signal quenching or, worse, reactions with the analyte.[2, 6] In dissolution DNP (d-DNP) experiments, rapid removal of the radicals from the hyperpolarized solution is desirable both for the sake of biocompatibility and to avoid rapid nuclear relaxation leading to losses of signal enhancement.[7]

Some attempts to alleviate these problems have recently been made by sequestering the radicals in micelles[8] or cryptands,[9] hiding the substrate in pores that are too small for the radical to enter,[10] or shielding the radicals in dendritic structures.[11] However, while they can be efficient when applicable, none of these solutions are general, and all have drawbacks.

Mesostructured silica materials[12] have emerged as an alternative strategy to alleviate these limitations. For instance, the use of mesoporous silica materials containing radicals that are regularly distributed at their pore surface obviates the use of a glassing agent to polarize an analyte in pure water because the porous structure prevents solvent crystallization and aggregation of radicals (Figure 1).[13] Another example is the use of mesoporous silica in MAS DNP to avoid segregation between radicals and colloids upon cooling.[14] However, in both systems the radical remains in close contact with the analyte and in the second case the approach requires the use of a solvent in which the radical is soluble. Recent work has also shown that radicals could be introduced within the silica matrix via a sol-gel process using a bis-silylated organic moiety that can generate radicals, thus providing a polarizing matrix for MAS DNP, though the localization of the radicals in the silica

[*] Dr. D. L. Silverio, Dr. T. C. Ong, Dr. M. Yulikov, Prof. G. Jeschke, Prof. C. Copéret
Dept. of Chemistry and Applied Biosciences, ETH Zürich
Vladimir-Prelog-Weg 1–5, 8093 Zürich (Switzerland)
E-mail: ccoperet@ethz.ch

[*] Dr. H. A. van Kalkeren, Dr. D. Baudouin, Dr. M. Cavailles, L. Veyre, Dr. C. Thieuleux
Université de Lyon, Institut de Chemie de Lyon, UMR C2P2 CNRS, Université de Lyon 1-ESCPE Lyon
43 Bd du 11 Novembre 1918, 69616 Villeurbanne (France)

P. Berruyer, Dr. S. Chaudhari, Dr. D. Gajan, Dr. A. Lesage, Dr. S. Jannin
Université de Lyon, Institut des Sciences Analytiques
CRMN CNRS-ENS Lyon-UCBL, 69100 Villeurbanne (France)

Dr. M. Baudin, Dr. S. Jannin, B. Vuichoud, A. Bornet, Prof. G. Bodenhausen, Prof. L. Emsley
Institut des Sciences et Ingénierie Chimiques, Ecole Polytechnique Fédérale de Lausanne (EPFL), 1015 Lausanne (Switzerland)

Dr. M. Baudin, Prof. G. Bodenhausen
Département de Chimie, Ecole Normale Supérieure, PSL Research University, UPMC Univ Paris 06, CNRS, Laboratoire des Biomolecules (LBM), 24 rue Lhomond, 75005 Paris (France)

Dr. M. Baudin, Prof. G. Bodenhausen
Sorbonne Universités, UPMC Univ Paris 06, Ecole Normale Supérieure, CNRS, Laboratoire des Biomolecules (LBM), Paris (France)

Supporting information for this article is given via a link at the end of the document.

matrix and their shielding from the analyte were not investigated.[15]

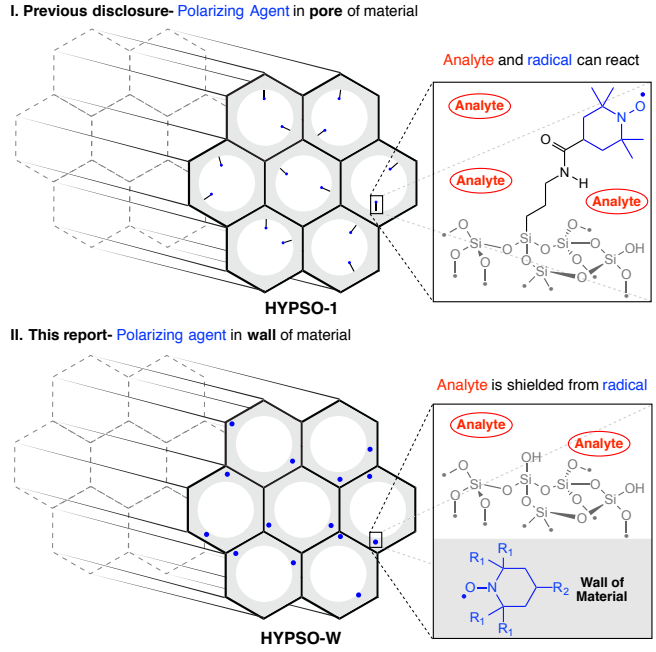

Figure 1. Comparison of materials with radicals in the pores, **HYPSO-1**, with materials with radicals in the walls, **HYPSO-W**.

We reasoned that hybrid mesostructured materials containing radicals embedded in the silica walls (Figure 1 bottom and Figure 2a) [12, 16] could provide a powerful approach to isolate the radical from the analyte, avoiding possible reactions and signal bleaching, while still removing the restriction to specific solvents or diluting the analyte in a co-solvent mixture. We report here the development of a HYPSO material containing radicals in the walls of the material (**HYPSO-W**) through a template approach and demonstrate its efficiency for MAS-DNP and d-DNP experiments. In particular, we show how engineering the wall structure and its composition by introducing organic functionalities significantly improve the polarization properties.

First, using **1**, a tris-silylated precursor containing a nitroxide radical (see ESI), and various amount (X) of $Si(OEt)_4$, the corresponding HYPSO material (**HYPSO-W1 [1/X]**) was prepared by a sol-gel process using Pluronic 123® (P123) and NaF as structure-directing agent and catalyst, respectively.[17] Optimal removal of P123 was achieved by washing with pyridine•HCl.[18] Using these protocols, a broad range of radical concentrations from 0.022 to 0.11 mmol/g (as determined by EPR; 49 to 58% yield) could be introduced into the silica matrix. We also synthesized materials **HYPSO-W2** that contain bis(triethoxysilyl)ethane **2** (Figure 2a, bottom), as an organic dopant to help polarization transfer via ^1H-^1H spin diffusion from the radicals to the pores.[21] **HYPSO-W2 [Y/1]** materials were all synthesized with the same 1/200 ratio of **1** to Si, but with varying content of the organic dopant **2** as defined by [Y/1] = [$Si(OEt)_4$/**2**].

All materials **HYPSO-W1** and **HYPSO-W2** have large pore volumes (0.7 to 1.2 cm^3/g), high surface areas (673 to 1066 m^2/g), narrow pore size distributions (5 to 9 nm) and large wall thicknesses (3 to 6 nm). These properties allow them to enclose the radical **1** (molecular diameter of ca. 2 nm) and to polarize a large volume of analyte. The SA-XRD diffraction patterns complemented by Transmission Electron Microscopy (TEM) are consistent with an ordered hexagonal structure of the porous network for all materials except **HYPSO-W2 [2/1]**, where the pattern is more indicative of a "wormlike" structure. The radical distribution was evaluated by EPR: decreasing the radical concentration leads to a narrowing of the EPR linewidth (13.1 G for **HYPSO-W1 [1/75]** to 12.3 G for **HYPSO-W1 [1/400]**) and an increase in the mean electron inversion recovery time ($<T_{1e}>$) from 32 µs for **HYPSO-W1 [1/75]** to 210 µs for **HYPSO-W1 [1/400]**. Both trends agree with an increasing average radical-radical distance with decreasing concentration.[13a, 22] For **HYPSO-W2**, $<T_{1e}>$ and line width are essentially unaffected by varying the concentration of bis-siloxyethane **2** (see ESI).

The ^1H enhancement (ε) of the solvent peak in MAS-DNP for materials impregnated with a 4:1 mixture of D_2O:H_2O did not change significantly with decreasing radical concentration from 0.11 to 0.045 mmol/g, staying at ca. 50-55 (Figure 2b), in contrast to 25 for **HYPSO-1** under the same conditions. Going to an even lower concentration, the enhancement drops but still remains at reasonable levels, *i.e.*, ε = 34 for **HYPSO-W1 [1/300]** and 22 for **HYPSO-W1 [1/400]**. Since the enhancements

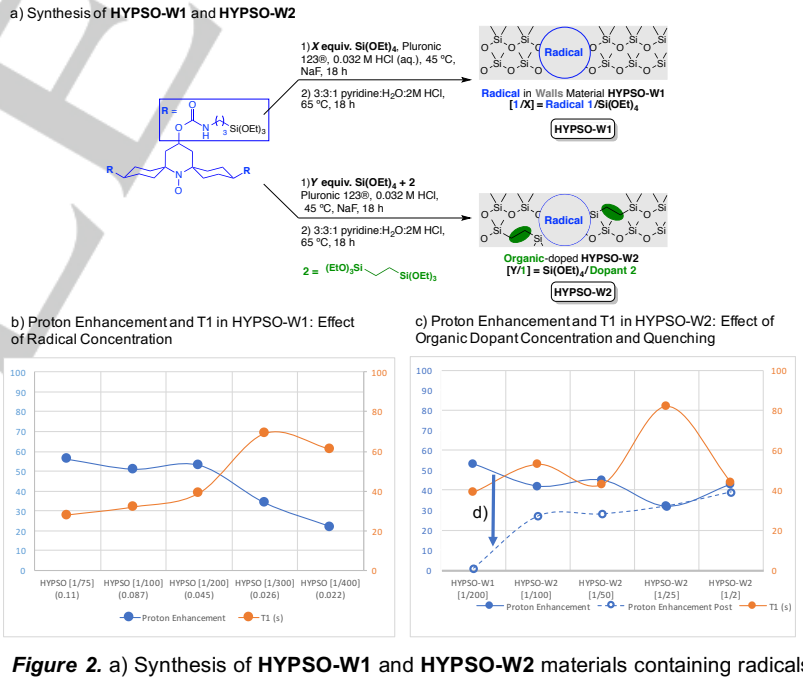

Figure 2. a) Synthesis of **HYPSO-W1** and **HYPSO-W2** materials containing radicals in the walls. MAS DNP performance (Proton enhancement (blue circles) and T_1 (orange circle) of b) **HYPSO-W1,** c) **HYPSO-W2** and d) **HYPSO-W2** and **HYPSO-W1** after treatment with ascorbic acid. All enhancements are determined at 600 MHz proton frequency (14.1 T) and ~100 K with 10 kHz MAS using 4:1 D_2O:H_2O as a solvent. T1 determined by a saturation recovery experiment. See ESI for details.

observed with **HYPSO-W1 [1/75]** to **[1/200]** are approximately the same, we chose **HYPSO-W1 [1/200]** as the optimal material, since lower concentrations of radicals should lead to a lower quenching factors.[23] Compared with **HYPSO-W1 [1/200]** (Figure 2c), all **HYPSO-W2** materials afforded approximately the same levels of enhancement, with **HYPSO-W2 [25/1]** giving somewhat lower enhancements due to its lower concentration in radicals (See ESI for details).

Notably **HYPSO-W1 [1/200]** yields effective MAS-DNP enhancements in solvents in which traditional polarizing agents like TEKPol[24] and AMUPol[25] are poorly soluble, as well as solvents that are poor at forming glasses (Figure 3), properties that, as mentioned above, are generally detrimental for DNP. Examination of the enhancement afforded by **HYPSO-W1 [1/200]** for a mixture of D_2O:H_2O at different magnetic fields reveals an enhancement ε = 100 at 9.4 T (400 MHz proton frequency). An enhancement ε = 20 is obtained at 18.8 T (800 MHz proton frequency, entries 7 and 8), an expected decrease with increasing field strength for DNP processes dominated by the cross effect.[2a, 26] Overall, this material is nearly twice as effective as state-of-the-art radical-containing materials for polarization[13, 15] in particular at high magnetic fields.[26]

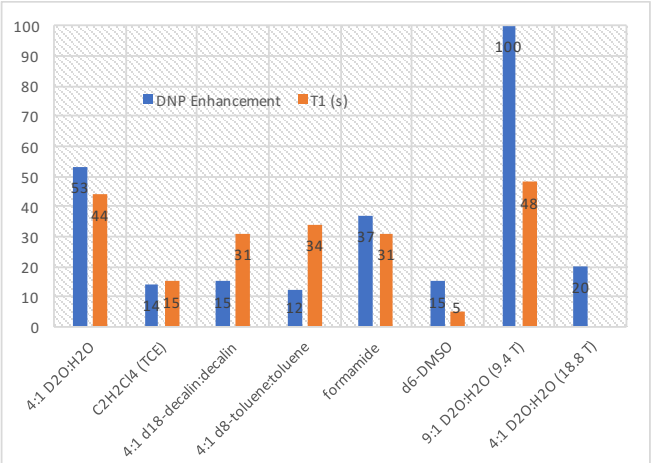

Figure 3. MAS-DNP enhancement (ε) in various solvents and at various magnetic field strengths with **HYPSO-W1 [1/200]**. Enhancements determined at given magnetic field at ~100 K. T_1 determined by saturation recovery. At 9.4 T, D_2O ; H_2O = 4:1 gave a lower ^1H enhancement of 71 in this case, although there was no difference in enhancement between these two solvent ratios at 14.1 T.

To probe how well the radicals in the **HYPSO-W** materials are shielded from the analytes, we first treated **HYPSO-W1 [1/200]** with a solution of ascorbic acid (known to reduce even sterically hindered nitroxide radicals),[27] and determined the resulting radical loading by EPR (Figure S1a). The ascorbic acid treatment resulted in only a 36% decrease of radical content. For comparison, this treatment was applied to **HYPSO-1,** a material with comparable physical features but with the radical localized at the pore surface, resulting in complete destruction of the radicals according to EPR (Figure S1b). However, both ascorbic acid-treated materials gave essentially no enhancement in the DNP experiment (Figure S1a). The poor enhancement in **HYPSO-W1** treated with ascorbic acid indicates that the remaining radicals are probably too deeply embedded to contribute to the polarization of the molecules present in the pores.

We therefore examined the polarization properties of **HYPSO-W1** and the organic doped **HYPSO-W2** materials (Figure 2d – opened circles). First, the decrease in radical content upon reaction with ascorbic acid is lower for **HYPSO-W2** than for **HYPSO-W1 [1/200]** (decrease of 22% vs. 36%). Second, and more importantly, these treated **HYPSO-W2 [100/1]** materials still afford a ^1H enhancement of 27 at 600 MHz, a mere 36% decrease with respect to its untreated form. When increasing the ratio of **2**/Si(OEt)$_4$ to 1/25, no loss of enhancement is observed after treatment. Overall the introduction of organic functionalities in the wall clearly helps to protect the radicals and to transfer the polarization from the radicals to the solvent molecules in the pores.

With these promising results, the **HYPSO-W** materials were also tested in dissolution DNP using pyruvic acid as a prototypical metabolite,[3b, 3d, 4, 28] which is known to reduce nitroxide radicals, so that previous nitroxide-containing materials failed to give rise to any polarization in d-DNP.

Dissolution-DNP experiments were carried out in a polarizer[29] operating at 1.2 K and 6.7 T equipped for cross polarization at low temperatures.[30] The optimal material is **HYPSO-W2 [25/1]**, which affords a polarization $P(^1H)$ = 39.5% for neat pyruvic acid with $\tau_{DNP}(^1H)$ = 20 minutes, resulting in $P(^{13}C)$ ~17% in about 60 minutes after ascorbic acid treatment. By comparison, a trityl-containing material, compatible with neat pyruvic acid, requires a much longer polarization time of 105 minutes.[13b] The corresponding **HYPSO-W1 [1/200]**, which lacks the ethyl fragments in its walls, affords a polarization of only $P(^1H)$ = 22.4% with $\tau_{DNP}(^1H)$ = 13 minutes. While ethyl groups are not mandatory to polarize the frozen solutions in the pores, their presence is very beneficial as it significantly boosts the polarization rates and improves the overall maximum polarization attained.

In conclusion, the introduction of electron polarization sources in the walls of mesostructured materials, dubbed **HYPSO-W** yield the highest enhancements in MAS-DNP for HYPSO materials, and are amenable to performing DNP in a wide variety of solvents. Importantly, **HYPSO-W** materials enable polarization of substrates in solution that would otherwise react with the nitroxides in conventional DNP formulations, e.g. neat pyruvic acid, combining the fast polarization buildup of nitroxide radicals and the stability of embedded nitroxide radicals. One critical aspect is the engineering of the structure of the material via incorporation of organic functionalities in the wall allowing more effective polarization transfer to the analyte.

Acknowledgements

We acknowledge the SNF for the 600 MHz DNP spectrometer (206021_150710). This work was supported by the Swiss National Science Foundation (SNF), ETH Zürich, the Ecole Polytechnique Fédérale de Lausanne, Bruker BioSpin Switzerland AG, ERC Advanced Grant No. 320860 and

EQUIPEX contract ANR-10-EQPX-47-01, and the ERC Advanced Grant "Dilute para-water". Mr. Wei-Chih Liao, Mr. Tigran Margossian, Ms. Laura Piveteau, and Dr. Martin Schwarzwälder are acknowledged for many useful discussions.

Author Contributions: D.L.S, C.C., C.T., S.J., T.C.O., and L.E. prepared the manuscript. D.L.S. developed and synthetized the HYPSO materials. H.A.v.K. developed the synthesis of radical **1**. T.C.O., D.L.S., P.B., S.C., D.G., A.L., L.E. developed and carried out the MAS-DNP experiments. M. B., D.B., M.C., carried out the d-DNP experiments. D.L.S., M.Y., L.V., and G.J. characterized the materials. S.J. and A.B. developed the d-DNP spectrometers. A.L. C.C., C.T., D.B., G.B., H.A.v.K., L.E. and S.J. conceived the project.

Keywords: magic angle spinning dynamic nuclear polarization • mesostructured silica • dissolution dynamic nuclear polarization • hybrid organic-inorganic materials

[1] a) B. A. Barnes, G. De Paëpe, A. P. C. van der Wel, K. N. Hu, C. G. Joo, S. V. Bajaj, L. M. Mak-Jurkauskas, R. J. Sirigiri, J. Herzfeld, J. R. Temkin, G. R. Griffin, *Appl. Magn. Reson.* **2008**, *34*, 237–263; b) M. Lelli, D. Gajan, A. Lesage, M. A. Caporini, V. Vitzthum, P. Miéville, F. Héroguel, F. Rascón, A. Roussey, C. Thieuleux, M. Boualleg, L. Veyre, G. Bodenhausen, C. Copéret, L. Emsley, *J. Am. Chem. Soc.* **2011**, *133*, 2104–2107.

[2] a) T. Maly, G. T. Debelouchina, V. S. Bajaj, K.-N. Hu, C.-G. Joo, M. L. Mak–Jurkauskas, J. R. Sirigiri, P. C. A. van der Wel, J. Herzfeld, R. J. Temkin, R. G. Griffin, *J. Chem. Phys.* **2008**, *128*, 052211; b) Q. Z. Ni, E. Daviso, T. V. Can, E. Markhasin, S. K. Jawla, T. M. Swager, R. J. Temkin, J. Herzfeld, R. G. Griffin, *Acc. Chem. Res.* **2013**, *46*, 1933–1941.

[3] a) J. H. Ardenkjær-Larsen, B. Fridlund, A. Gram, G. Hansson, L. Hansson, M. H. Lerche, R. Servin, M. Thaning, K. Golman, *Proc. Natl. Acad. Sci. U. S. A.* **2003**, *100*, 10158–10163; b) R. E. Hurd, Y.-F. Yen, A. Chen, J. H. Ardenkjaer-Larsen, *J. Magn. Reson. Im.* **2012**, *36*, 1314–1328; c) A. J. Rossini, A. Zagdoun, M. Lelli, A. Lesage, C. Copéret, L. Emsley, *Acc. Chem. Res.* **2013**, *46*, 1942–1951; d) J. H. Ardenkjaer-Larsen, *J. Magn. Reson.* **2016**, *264*, 3–12.

[4] F. A. Gallagher, M. I. Kettunen, K. M. Brindle, *Prog. Nucl. Magn. Reson. Spectrosc.* **2009**, *55*, 285–295.

[5] a) S. J. Nelson, J. Kurhanewicz, D. B. Vigneron, P. E. Z. Larson, A. L. Harzstark, M. Ferrone, M. van Criekinge, J. W. Chang, R. Bok, I. Park, G. Reed, L. Carvajal, E. J. Small, P. Munster, V. K. Weinberg, J. H. Ardenkjaer-Larsen, A. P. Chen, R. E. Hurd, L.-I. Odegardstuen, F. J. Robb, J. Tropp, J. A. Murray, *Sci. Transl. Med.* **2013**, *5*, 198ra108; b) S. J. Nelson, J. Kurhanewicz, D. B. Vigneron, P. E. Z. Larson, A. L. Harzstark, M. Ferrone, M. van Criekinge, J. W. Chang, R. Bok, I. Park, G. Reed, L. Carvajal, E. J. Small, P. Munster, V. K. Weinberg, J. H. Ardenkjaer-Larsen, A. P. Chen, R. E. Hurd, L.-I. Odegardstuen, F. J. Robb, J. Tropp, J. A. Murray, *Sci. Transl. Med.* **2013**, *5*, 198ra108.

[6] T.-C. Ong, M. L. Mak-Jurkauskas, J. J. Walish, V. K. Michaelis, B. Corzilius, A. A. Smith, A. M. Clausen, J. C. Cheetham, T. M. Swager, R. G. Griffin, *J. Phys. Chem. B* **2013**, *117*, 3040–3046.

[7] a) P. Miéville, S. Jannin, G. Bodenhausen, *J. Magn. Reson.* **2011**, *210*, 137–140; b) P. Miéville, P. Ahuja, R. Sarkar, S. Jannin, P. R. Vasos, S. Gerber-Lemaire, M. Mishkovsky, A. Comment, R. Gruetter, O. Ouari, P. Tordo, G. Bodenhausen, *Angew. Chem. Int. Ed.* **2010**, *49*, 6182–6185.

[8] a) K. G. Valentine, G. Mathies, S. Bédard, N. V. Nucci, I. Dodevski, M. A. Stetz, T. V. Can, R. G. Griffin, A. J. Wand, *J. Am. Chem. Soc.* **2014**, *136*, 2800–2807; b) M. Lelli, A. J. Rossini, G. Casano, O. Ouari, P. Tordo, A. Lesage, L. Emsley, *Chem. Commun.* **2014**, *50*, 10198–10201.

[9] J. Mao, D. Akhmetzyanov, O. Ouari, V. Denysenkov, B. Corzilius, J. Plackmeyer, P. Tordo, T. F. Prisner, C. Glaubitz, *J. Am. Chem. Soc.* **2013**, *135*, 19275–19281.

[10] E. Pump, J. Viger-Gravel, E. Abou-Hamad, M. K. Samantaray, B. Hamzaoui, A. Gurinov, D. H. Anjum, D. Gajan, A. Lesage, A. Bendjeriou-Sedjerari, L. Emsley, J.-M. Basset, *Chem. Sci.* **2017**, DOI:10.1039/C1036SC02379G.

[11] W.-C. Liao, T.-C. Ong, D. Gajan, F. Bernada, C. Sauvee, M. Yulikov, M. Pucino, R. Schowner, M. Schwarzwalder, M. R. Buchmeiser, G. Jeschke, P. Tordo, O. Ouari, A. Lesage, L. Emsley, C. Coperet, *Chem. Sci.* **2016**, DOI: 10.1039/C1036SC03139K.

[12] a) R. J. P. Corriu, A. Mehdi, C. Reye, *J. Mater. Chem.* **2005**, *15*, 4285–4294; b) F. Hoffmann, M. Cornelius, J. Morell, M. Fröba, *Angew. Chem. Int. Ed.* **2006**, *45*, 3216–3251.

[13] a) D. Gajan, M. Schwarzwälder, M. P. Conley, W. R. Grüning, A. J. Rossini, A. Zagdoun, M. Lelli, M. Yulikov, G. Jeschke, C. Sauvée, O. Ouari, P. Tordo, L. Veyre, A. Lesage, C. Thieuleux, L. Emsley, C. Copéret, *J. Am. Chem. Soc.* **2013**, *135*, 15459–15466; b) D. Gajan, A. Bornet, B. Vuichoud, J. Milani, R. Melzi, H. A. van Kalkeren, L. Veyre, C. Thieuleux, M. P. Conley, W. R. Grüning, M. Schwarzwälder, A. Lesage, C. Copéret, G. Bodenhausen, L. Emsley, S. Jannin, *Proc. Natl. Acad. Sci. U. S. A.* **2014**, *111*, 14693–14697; c) D. Baudouin, H. A. van Kalkeren, A. Bornet, B. Vuichoud, L. Veyre, M. Cavailles, M. Schwarzwalder, W. C. Liao, D. Gajan, G. Bodenhausen, L. Emsley, A. Lesage, S. Jannin, C. Coperet, C. Thieuleux, *Chem. Sci.* **2016**, DOI: 10.1039/C1036SC02055K; d) W. R. Grüning, H. Bieringer, M. Schwarzwälder, D. Gajan, A. Bornet, B. Vuichoud, J. Milani, D. Baudouin, L. Veyre, A. Lesage, S. Jannin, G. Bodenhausen, C. Thieuleux, C. Copéret, *Helv. Chim. Acta* **2016**, DOI: 10.1002/hlca.201600122.

[14] L. Piveteau, T.-C. Ong, A. J. Rossini, L. Emsley, C. Copéret, M. V. Kovalenko, *J. Am. Chem. Soc.* **2015**, *137*, 13964–13971.

[15] E. Besson, F. Ziarelli, E. Bloch, G. Gerbaud, S. Queyroy, S. Viel, S. Gastaldi, *Chem. Commun.* **2016**, *52*, 5531–5533.

[16] a) G. Dubois, R. J. P. Corriu, C. Reye, S. Brandes, F. Denat, R. Guilard, *Chem. Commun.* **1999**, 2283-2284; b) O. Olkhovyk, M. Jaroniec, *J. Am. Chem. Soc.* **2005**, *127*, 60–61.

[17] a) P. Schmidt-Winkel, P. Yang, D. I. Margolese, B. F. Chmelka, G. D. Stucky, *Adv. Mater.* **1999**, *11*, 303–307; b) R. J. P. Corriu, A. Mehdi, C. Reye, C. Thieuleux, *Chem. Commun*. **2002**, 1382-1383.

[18] A. Boullanger, J. Alauzun, A. Mehdi, C. Reye, R. J. P. Corriu, *New J. Chem.* **2010**, *34*, 738–743.

[19] D. Zhao, J. Feng, Q. Huo, N. Melosh, G. H. Fredrickson, B. F. Chmelka, G. D. Stucky, *Science* **1998**, *279*, 548–552.

[20] Y. Ma, C. Loyns, P. Price, V. Chechik, *Org. Biomol. Chem.* **2011**, *9*, 5573–5578.

[21] a) P. C. A. van der Wel, K.-N. Hu, J. Lewandowski, R. G. Griffin, *J. Am. Chem. Soc.* **2006**, *128*, 10840–10846; b) A. J. Rossini, A. Zagdoun, F. Hegner, M. Schwarzwälder, D. Gajan, C. Copéret, A. Lesage, L. Emsley, *J. Am. Chem. Soc.* **2012**, *134*, 16899–16908.

[22] K.-N. Hu, H.-h. Yu, T. M. Swager, R. G. Griffin, *J. Am. Chem. Soc.* **2004**, *126*, 10844–10845.

[23] A. J. Rossini, A. Zagdoun, M. Lelli, D. Gajan, F. Rascon, M. Rosay, W. E. Maas, C. Coperet, A. Lesage, L. Emsley, *Chem. Sci.* **2012**, *3*, 108–115.

[24] A. Zagdoun, G. Casano, O. Ouari, M. Schwarzwälder, A. J. Rossini, F. Aussenac, M. Yulikov, G. Jeschke, C. Copéret, A. Lesage, P. Tordo, L. Emsley, *J. Am. Chem. Soc.* **2013**, *135*, 12790–12797.

[25] C. Sauvée, M. Rosay, G. Casano, F. Aussenac, R. T. Weber, O. Ouari, P. Tordo, *Angew. Chem. Int. Ed.* **2013**, *52*, 10858–10861.

[26] G. Mathies, M. A. Caporini, V. K. Michaelis, Y. Liu, K.-N. Hu, D. Mance, J. L. Zweier, M. Rosay, M. Baldus, R. G. Griffin, *Angew. Chem. Int. Ed.* **2015**, *54*, 11770–11774.

[27] J. T. Paletta, M. Pink, B. Foley, S. Rajca, A. Rajca, *Org. Lett.* **2012**, *14*, 5322–5325.

[28] S. E. Day, M. I. Kettunen, F. A. Gallagher, D. E. Hu, M. Lerche, J. Wolber, K. Golman, J. H. Ardenkjaer-Larsen, K. M. Brindle, *Nat. Med.* **2007**, *13*, 1382–1387.

[29] A. Comment, B. van den Brandt, K. Uffmann, F. Kurdzesau, S. Jannin, J. A. Konter, P. Hautle, W. T. Wenckebach, R. Gruetter, J. J. van der Klink, *Concepts Magn. Reson. B* **2007**, *31B*, 255–269.

[30] a) S. Jannin, A. Bornet, S. Colombo, G. Bodenhausen, *Chem. Phys. Lett.* **2011**, *517*, 234–236; b) S. Jannin, A. Bornet, R. Melzi, G. Bodenhausen, *Chem. Phys. Lett.* **2012**, *549*, 99–102; c) A. Bornet, R. Melzi, A. J. Perez Linde, P. Hautle, B. van den Brandt, S. Jannin, G. Bodenhausen, *J. Phys. Chem. Lett.* **2013**, *4*, 111–114.

Entry for the Table of Contents

COMMUNICATION

Walls can talk. Hybrid materials containing nitroxide radicals embedded in the walls can polarize analytes efficiently while being protected by inorganic silica, thus leading to efficient polarization matrices for solid state and dissolution DNP.

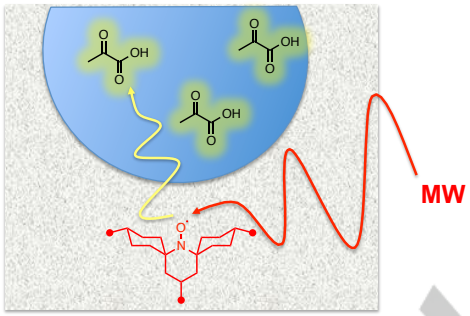

D. L. Silverio, H. A. van Kalkeren, T.-C. Ong, M. Baudin, M. Yulikov, L. Veyre, P. Berruyer, S. Chaudhari, D. Gajan, D. Baudouin, M. Cavaillès, B. Vuichoud, A. Bornet, G. Jeschke, G. Bodenhausen, A. Lesage, L. Emsley, S. Jannin, C. Thieuleux, and C. Copéret**

Page No. – Page No.

Tailored Polarizing Hybrid Solids with Nitroxide Radicals Localized in Mesostructured Silica Walls

Electronic Supplementary Information

Tailored Polarizing Hybrid Solids with Nitroxide Radicals Localized in Mesostructured Silica Walls.

General Experimental Details: All synthetic reactions, work up procedures, and purifications were carried out without taking special precaution to exclude air and moisture, unless otherwise noted. All solvents used in work up and purification were ACS grade and were not purified prior to use, with the exception of water, which was deionized. All aqueous solutions were made with deionized water.

Experimental Details for Instrumentation and Measurements:

Continuous Wave EPR Spectroscopy (CW EPR)

Continuous Wave (CW) EPR spectra were recorded on a Bruker EMX X Band spectrometer (9.5 GHz microwave frequency). Conversion time was set to 40.96 ms, time constant to 5.12 ms respectively and 1024 data points were recorded. The modulation frequency was 100 kHz and the modulation amplitude 1 G. In all measurements, attenuation was varied such that no saturation was observed.

Spin Count

The samples were filled in Hirschmann glass capillaries, which were then closed with putty. The spectra were recorded at room temperature and with a sweep width of 600 G and attenuation between 26 and 14 dB. The amount of radical was determined by double integration of the CW spectra and referencing to a calibration curve of TEMPO ((2,2,6,6-Tetramethylpiperidin-1-y)oxyl) solutions measured for the concentration range between 0.4 and 80 mM. EPR spectrum of sealant putty of the EPR tube was subtracted using the EasySpin program in MATLAB®(R2011b, MathWorks Inc.). An additional correction for the difference in the incident microwave power has been taken into account. Data was processed with MATLAB®.

Peak-to-peak Linewidth

For each sample, the material was impregnated with 1,1,2,2-tetrachloroethane and filled in a 3.0 mm quartz tube. All spectra were recorded at 110 K using a nitrogen flow cryostat. Attenuation was varied from 32 to 23 dB. The EPR spectrum of a nitroxide radical consists of three lines due to strong hyperfine interaction with the ^{14}N nucleus. For the line-width measurements we have used the central line, which is less broadened by the *g*-tensor and hyperfine anisotropies and which therefore is the most sensitive to the dipolar broadening. For the obtained signal-to-noise ratios, the

estimated linewidth error bars were in the order of 5 %.

Pulse EPR Spectroscopy

EPR measurements were conducted at W band (94 GHz) on a Bruker Elexsys E680 EPR spectrometer at 105 K. Approximately 1 μL of each sample powder was put into a quartz capillary with 0.89/0.5 mm outer/inner diameter (Wilmad). To perform EPR relaxation measurements a capillary containing sample was frozen by immersion into liquid nitrogen and transferred to the EPR resonator, pre-cooled at 105 K. During the measurements the sample temperature was stabilized using an Oxford Instruments He-flow cryostat. The inversion recovery pulse sequence π-T_{mix}-π/2-τ-π-τ-echo with variable time T_{mix} was used to detect the recovery of the longitudinal magnetization. The variable delay Hahn echo sequence π/2-τ-π-τ-echo (variable delay time τ) was used to determine the phase memory times. Pulse lengths of 40 ns for π/2 pulses and 80 ns for π pulses were used.

Inversion recovery data were fitted using a stretched exponential decay function of the form $V(t) = V_0 + V_1 \cdot e^{-(t/T_1)^\beta}$. The values T_1, β, and $\langle T_{IR} \rangle = \int_0^\infty e^{-(t/T_1)^\beta} dt = \frac{T_1}{\beta} \cdot \Gamma\left(\frac{1}{\beta}\right)$ are reported in Table S3). The phase memory decay data were fitted using a mono-exponential decay function $V(t) = V_0 + V_1 \cdot e^{-t/T_2}$. Corresponding delay times are also presented in the Table S3.

Solution State NMR

Solution state ^{1}H NMR spectra were measured with a Bruker Avance III 300 MHz (7.0 T) spectrometer. Chemical shifts are reported as referenced to the solvent resonance of CD_3OD (δ 3.34 ppm). Data are reported as follows: chemical shift, multiplicity (t = triplet, m = multiplet), coupling constants (Hz), and integration. Solution state ^{13}C NMR spectra were measured with a Bruker Avance III 300 MHz (7.0 T) spectrometer with proton decoupling. Chemical shifts are reported as referenced to the solvent resonance of CD_3OD (δ 49.86 ppm). Peaks are singlets unless otherwise noted.

MAS-DNP Solid-State Spectroscopy

DNP enhanced solid-state NMR. DNP enhanced solid-state NMR experiments were conducted on a 600 MHz (14.1 T) spectrometer (Bruker Biospin) using a 3.2 mm HX or HXY probe located at ETH Zurich.[1] The sample is cooled to 100 K by a cryogenic heat exchanger system. Microwaves used to drive the DNP cross effect are provided by gyrotrons emitting at 395 GHz (600 MHz spectrometer) with power between 6 to 10 W. Ramped cross polarization (CP)[2] from ^{1}H to heteronuclei was used for all experiments with contact time between 0.5 to 2.0 ms. The DNP build-up time (T_B) was measured by saturation recovery,[3] and the recycling delay time was set to 1.3T_B. Potassium bromide (KBr) was used to calibrate the magic angle for the MAS probes.

DNP enhanced solid-state NMR experiments conducted at 400 MHz (9.4 T) have been recorded on a Bruker BioSpin Spectrometer located at the ISA-CRMN Lyon and equipped with Advance III HD console, a LT-MAS 3.2mm triple-resonance HXY probe (set to ^{13}C/^{15}N configuration with the proper

insert), gyrotron that provided continuous microwaves irradiation at 263 GHz. Sample temperature during experiment is approximately 100 K and the sample was spun at the magic angle at 8 kHz.
DNP enhanced solid-state NMR experiments conducted at 800 MHz (18.8 T) have been recorded on a Bruker BioSpin Spectrometer located at the ISA-CRMN Lyon and equipped with an Avance III console, a LT-MAS 3.2 mm triple-resonance HXY probe (set to $^{13}C/^{15}N$ configuration with the proper insert), gyrotron that provided continuous microwaves irradiation at 527 GHz. Sample temperature during experiment is approx. 100 K and the sample was spin at the magic angle at 8 kHz.
Sample Preparation for MAS-DNP with HYPSO materials. For determination of enhancement of **HYPSO-W** materials, 6.0–10.0 mg of silica material was weighed into a watch glass. Solvent was added by incipient wetness impregnation[4] using a solvent volume equal to three times (unless otherwise noted) the pore volume of the material (as determined be nitrogen adsorption-desorption; see below for details) in three portions and mixed with a glass stirring rod between additions. The impregnated material was packed into a 3.2 mm sapphire rotor and capped with a Teflon insert followed by a zirconia drive tip. The sample was then inserted into the spectrometer.
Sample Preparation for MAS-DNP with radical solution impregnated into mesoporous silica.
In accordance to a procedure in the literature,[5] a 32 mM solution of radical (either TEKPol or AMUPol) was prepared. Then, 6.0–10.0 mg of SBA-15 was weighed into a watch glass. Solvent (a 1:1 mixture of the radical solution and pure solvent) was added by incipient wetness impregnation[6] using a solvent volume equal to ~2.3 times the pore volume of the material in three portions and mixed with a glass stirring rod between additions. The impregnated material was packed in a 3.2 mm sapphire rotor and capped with a Teflon insert followed by a zirconia drive tip. The sample was then inserted into the spectrometer. For data related to this, please see Table S4.
To measure the enhancement in the absence of SBA-15, the solution (a 1:1 mixture of the radical solution and pure solvent) was added directly to the rotor and capped with a silicon plug followed by a zirconia drive tip. The sample was then inserted into the spectrometer.

Dissolution DNP Spectroscopy
The dissolution DNP polarizer consists of a 6.7 T (285.5 MHz) superconducting wide bore magnet from Oxford Instruments, equipped with a cryostat developed at PSI (Paul Scherrer Institut, Switzerland). This cryostat enables to work at liquid helium temperature (4.2 K) and down to 1.2 K when pumping on the helium bath.
A home-built NMR probe enables to monitor the polarization while shining microwaves directly on the sample cavity through a coaxial line. In the case of TEMPO, the microwave frequency is set to 188.3 GHz for negative DNP, and 187.9 GHz for positive DNP.
Sample preparation was performed by impregnating the HYPSO powder with a mixture of D_2O/H_2O (80/20) in order to fill 95 % of the pores. For the ^{13}C polarization experiments, neat pyruvic acid was used instead.

Calculation of Enhancement Factors (ε)
CP MAS DNP enhancement factors on the nucleus X (ε_X) were determined by scaling the intensities of the spectra of the nuclei X obtained under the same experimental conditions with or without μW irradiation. The microwave power was optimized (within the limits of the gyrotron) for each sample. The number of degassing steps (1-3) was optimized to get the highest enhancement for each solvent.[7]

Elemental Analysis
Carried out by Mikroelementaranalyse at ETH Zürich with a LECO TruSpec Micro taking the average of two measurements.

Infrared (IR) Spectroscopy
Measurements for hybrid materials were carried out on undiluted samples with a Bruker Alpha FT-IR spectrometer equipped with the DRIFT (Diffuse Reflectance Infrared Fourier Transform) module QuickSnap™ accessory. Bands are reported for λ_{max} in cm^{-1} from 1600 to 4000 cm^{-1} (lower wavenumbers become difficult to analyze due to silica saturation) and characterized as broad (br), strong (s), medium (m), or weak (w) relative to other bands from 1600 to 4000 cm^{-1}.

Nitrogen Adsorption-Desorption
Measurements were carried out at 77 K using a BELSORB-Mini from BEL-JAPAN. Before N_2 adsorption, the samples were degassed at less than 10^{-4} Torr at 408 K for at least 5 hours. Both the pore volume and the peak pore diameter were calculated using the Barrett–Joyner–Halenda (BJH) method. The specific surface area (S_{BET}) was calculated according to the Brunauer–Emmett–Teller (BET) equation. Calculations were carried out using the BEL-Master software package.

Small Angle X-ray Diffraction (SAXRD)
Small-Angle X-ray diffraction (SAXRD) on powder was carried out with a Bruker D8 Avance diffractometer (33 kV & 45 mA) with CuKα radiation (λ = 0.154 nm) in the Service Diffraction RX, IRCE Lyon, France. The diffraction patterns were collected in the 2θ angle range [0.45°-7.0°] at a scanning rate of 0.1°/min. The interplane spacings, d(hkl) for different Miller indices (hkl) were calculated using the Bragg's law ($nk = 2d\sin\theta$). The lattice parameter (a0) for the hexagonal structured mesoporous material is given by $a0 = 2d(100)/\sqrt{3}$.

Transmission Electron Microscopy
Measurements were done on a Philips CM12 (100 kV) equipped with CCD detector. The samples were prepared by shaking the dry sample with a Cu grid covered by a carbon film.

Reagents and Solvents for Reactions:

Amino Triketone S1 was prepared in accordance to a procedure in the literature.[8]

L-Ascorbic Acid was purchased from Aldrich and used as received.

Bis(triethoxylsilyl)ethane was purchased from ABCR and used as received.

Dibutyltin Dilaurate was purchased from Alfa Aesar and used as received.

Ethanol (denatured) was purchased from Aldrich and used as received.

Hydrogen Peroxide (30 wt% in H_2O) was purchased from EMD and used as received.

Methanol was purchased from Aldrich and used as received.

Pluronic® P-123 was purchased from Aldrich and used as received.

Potassium Carbonate was purchased from Aldrich and used as received.

SBA-15 was synthesized analogously to the **HYPSO-W1** materials, only radical **1** was replaced with three times the molar amount of $Si(OEt)_4$. As determined by analysis of the nitrogen adsorption-desorption isotherm (see above for details), surface area is 944 m^2/g, pore volume is 1.5 cm^3/g, peak pore diameter is 9.2 nm.

Sodium Borohydride was purchased from Aldrich and used as received.

Sodium Fluoride was purchased from ABCR and used as received.

Sodium Tungstate Dihydrate was purchased from Fluka and used as received.

Tetraethyl Orthosilicate ($Si(OEt)_4$) was purchased from Aldrich and used as received.

Tetrahydrofuran (HPLC grade, inhibitor free) was purchased from Aldrich and distilled under N_2 from sodium benzophenone ketyl prior to use.

3-(Triethoxysilyl)propyl Isocyanate was purchased from Aldrich and distilled under vacuum ($<10^{-4}$ Torr) to afford a clear, colorless oil that was stored under argon prior to use.

Solvents for NMR studies:

Decalin (D18, 99%) (cis/trans mixture) was purchased from Cambridge Isotope Laboratories and used as received.

Decalin (protio) (cis/trans mixture) was purchased from Acros and used as received.

Deuterium Oxide (**D_2O, 99%)** was purchased from Aldrich and used as received.

Dimethyl Sulfoxide (D6, 99.9%) was purchased from Cambridge Isotope Laboratories and used as received.

Formamide was purchased from Aldrich and used as received.

Methanol (D4, 99.8%) was purchased from Cambridge Isotope Laboratories and used as received.

1,1,2,2-Tetrachloroethane was purchased from Fluka and used as received.

Toluene (D8, 99.5%) was purchased from Cambridge Isotope Laboratories and used as received.

Toluene (Methyl-D3, 98%) was purchased from Cambridge Isotope Laboratories and used as received.

Water was purified with a Milli-Q® water purifier to obtain Type 1 ultrapure water.

Scheme S1. Synthesis of radical **1**

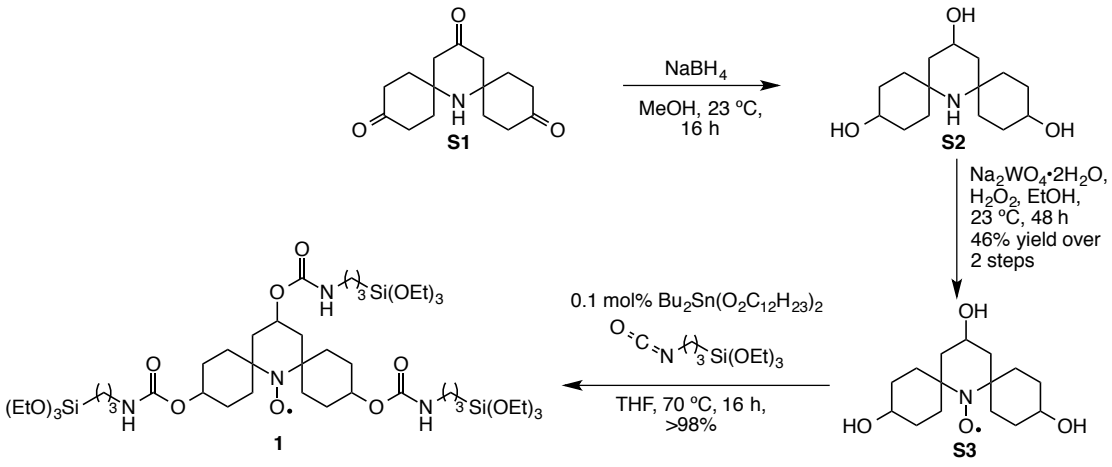

7-Azadispiro[5.1.5^8.3^6]hexadecane-3,11,15-triol (S2): Amino triketone **S1**[8] (4.40 g, 16.7 mmol) is added to a 500 mL round-bottom flask equipped with a stir bar and then dissolved in MeOH (170 mL). The reaction is cooled to 0 ºC and $NaBH_4$ (3.79 g, 100 mmol) is added in one portion. The mixture is allowed to stir at 23 ºC for 16 hours and is then quenched by the addition of acetone (30 mL) and H_2O (30 mL). The mixture is allowed to stir for an additional 30 min and then concentrated in a 1:1 mixture of CH_2Cl_2/MeOH (100 mL) is added and the mixture is filtrated to remove the majority of the salts. Concentration of the filtrate and subsequent column chromatography (20→50% MeOH in CH_2Cl_2) afforded **S2** (3.76 g, 14.0 mmol, 84% yield) as a colorless solid. ^{1}H NMR (300 MHz, CD_3OD): δ 3.95–3.86 (m, 1H), 3.66–3.52 (m, 2H), 2.05–1.29 (m, 18H), 1.02(t, *J* = 11.9 Hz, 2H); ^{13}C NMR (75 MHz, MeOD) δ 70.9, 65.3, 54.8, 48.8, 41.9, 35.4, 32.5, 32.0; HRMS (ESI$^+$) calcd. for $C_{15}H_{28}NO_3$ $[M+H]^+$ 270.2064, found 270.2063.

7-Azadispiro[5.1.5^8.3^6]hexadecane-3,11,15-trihydroxy-7-oxy (S3): Amino triol (**S2**, 3.65 g, 13.5 mmol) is added to a 500 mL round-bottom flask and dissolved with EtOH (140 mL). $Na_2WO_4{\cdot}2H_2O$ (615 mg, 1.86 mmol) is added in one portion and H_2O_2 (30% in H_2O, 34.0 mL) is added dropwise over approximately one hour to a stirring solution. The mixture is allowed to stir at 22 ºC for 48 h and then cooled to 0 ºC with an ice bath. K_2CO_3 (15.0 g, 109 mmol) is then added in small portions taking care not to let the temperature exceed 10 °C. The mixture is allowed to reach 22 ºC and the aqueous layer is extracted with $CHCl_3$ (2 × 100 mL). The combined organic layers are dried over Na_2SO_4 and concentrated in vacuo to afford an orange-red solid. Column chromatography (5 → 10% MeOH in CH_2Cl_2) affords **S3** (2.20 g, 7.74 mmol, 57.3% yield) as an orange powder following drying under high vacuum (10^{-4} Torr at 22 ºC for 12 h). IR (KBr) ν 3356, 2931, 2869, 1450 cm^{-1}; HRMS (ESI$^+$) calcd. for $C_{15}H_{26}NO_4Na$ $[M+Na]^+$ 307.1754, found 307.1755.

7-Azadispiro[5.1.5^8.3^6]hexadecane-3,11,15-triyl)tris((3-((triethoxysilyl) propyl)carbamoyl)oxy)-7-oxy (1): A 10 mL oven-dried Schlenk tube equipped with a oven-dried stir bar is brought into a glovebox and charged with radical **S3** (0.10 g, 0.35 mmol). The vessel is sealed with a rubber septum and electrical tape and brought outside the glovebox. Under an overpressure of Ar, tetrahydrofuran (5 mL), 3-(triethoxysilyl)propyl isocyanate (0.30 mL**,** 1.2 mmol) and dibutyltin dilaurate (5 µL, 9 µmol) are added via syringe in the stated order. The tube is sealed with a glass stopper and heated to 70 °C while being allowed to stir for 16 h. The radical dissolves after approximately one hour to give an orange-red solution. After allowing the vessel to cool to 22 ºC, the solution is transferred to a round-bottomed flask using ethyl acetate and the solution is concentrated in vacuo to afford a red oil. The product is quickly purified by flash column chromatography (21 mm column, ~10g Si gel, 150 mL 3:1 petroleum ether:ethyl acetate followed by 150 mL ethyl acetate; column time <5 minutes) to afford **1** (0.36 mg, 0.35 mmol, >98% yield) as a red oil. IR (KBr) ν 3340, 2974, 2929, 2884, 1720, 1698, 1529; HRMS (ESI$^+$) calcd. for $C_{45}H_{89}NO_{16}Si_3Na$ $[M+Na]^+$ 1048.5474, found 1048.5451.

Synthesis of HYPSO-W1 Materials:

HYPSO-W1 [1/75] [1/75 dilution of radical to $Si(OEt)_4$]: A 50 mL wide-mouth PET bottle equipped with a stir bar is charged with 480 mg (~0.082 mmol) Pluronic® P-123 followed by 20 mL of a pH = 1.5 (0.032 M) aqueous solution of HCl. The bottle is sealed with a cap, and the solution is allowed to stir at 23 ºC at 400 RPM for 3 hours until complete dissolution of Pluronic® P-123 is achieved. A homogenous solution of $Si(OEt)_4$ (1.25 mL, 5.60 mmol) and radical **1** (77 mg, 0.075 mmol) is then added in one portion, and the pale red solution is allowed to stir at 23 ºC for one hour. The stirring solution is heated to 45 ºC at which point 8.9 mg (0.21 mmol) of NaF is added. An off-white precipitate forms within 30 minutes and this suspension is allowed to stir at 400 RPM and 45 ºC for 18 hours. The precipitate is collected on a porosity 3 glass-fritted funnel and washed with deionized water (3 x 20 mL), acetone (3 x 20 ml), and dichloromethane (1 x 20 mL). To remove the surfactant, the solid is then transferred to a 50 mL round bottomed flask containing a stir bar as well as a premixed solution of pyridine (3.75 mL), deionized water (3.75 mL), and a 2 M aqueous solution of HCl (1.25 mL). The reaction vessel is capped with a rubber septum containing a vent needle and allowed to stir at 65 ºC for 18 h. After allowing the vessel to cool to room temperature, the solid is collected on a porosity 3 glass-fritted funnel and washed with deionized water (3 x 20 mL), acetone (3 x 20 ml), and pentanes (3 x 20 mL). The solid is then dried for 12 hours under vacuum (10^{-4} Torr) at 135 ºC using a temperature ramp of 1 ºC/min from room temperature (~23 ºC), and then brought into a glovebox. Following drying, 345 mg of a light yellow solid is obtained. IR (DRIFT): 3735 (w), 3436 (w, br), 2936 (w), 2877 (w), 1818 (w, br), 1745 (m), 1716 (s), 1703 (s) cm^{-1}. Elemental analysis: C = 8.78%$_{wt}$; H = 2.00%$_{wt}$; N =1.02%$_{wt}$.

HYPSO-W1 [1/100] [1/100 dilution of radical to $Si(OEt)_4$]: Prepared analogously to **HYPSO-W1 [1/75]** using 319 mg of Pluronic® P-123, 13.2 mL of pH = 1.5 aqueous HCl, 0.84 mL (3.7 mmol) $Si(OEt)_4$, 39 mg (0.075 mmol) of radical **1**, and 5.9 mg (0.14 mmol) of NaF to afford 214 mg of **HYPSO-W1 [1/100]** as a pale yellow solid. IR (DRIFT): 3737 (w), 3461 (w, br), 2955 (w), 2852 (w), 1870 (w, br), 1717 (s), 1703 (s), 1692 (s) cm^{-1}. Elemental analysis: C = 4.77%$_{wt}$; H = 1.67%$_{wt}$; N =0.62%$_{wt}$.

HYPSO-W1 [1/200] [1/200 dilution of radical to $Si(OEt)_4$]: Prepared analogously to **HYPSO-W1 [1/75]** using 638 mg of Pluronic® P-123, 26.4 mL of pH = 1.5 aqueous HCl, 1.67 mL (7.46 mmol) $Si(OEt)_4$, 39 mg (0.038 mmol) of radical **1**, and 12 mg (0.28 mmol) of NaF to afford 440 mg of **HYPSO-W1 [1/200]** as a pale yellow solid. IR (DRIFT): 3734 (w), 3469 (m, br), 2973 (m), 2933 (m), 2897 (m), 2872 (m), 1852 (w, br), 1735 (m), 1709 (s), 1696 (s) cm^{-1}. Elemental analysis: C = 4.30%$_{wt}$; H = 1.59%$_{wt}$; N =0.39%$_{wt}$.

HYPSO-W1 [1/300] [1/300 dilution of radical to $Si(OEt)_4$]: Prepared analogously to **HYPSO-W1 [1/75]** using 638 mg of Pluronic® P-123, 26.4 mL of pH = 1.5 aqueous HCl, 1.67 mL (7.46 mmol) $Si(OEt)_4$, 25 mg (0.025 mmol)

of radical **1**, and 12 mg (0.28 mmol) of NaF to afford 414 mg of **HYPSO-W1 [1/300]** as an off-white solid. IR (DRIFT): 3739 (m), 3535 (w, br), 2974 (w), 2937 (w), 2882 (w), 1862 (m, br), 1743 (m), 1710 (s), 1700 (s) cm^{-1}. Elemental analysis: C = 3.68%$_{wt}$; H = 1.25%$_{wt}$; N =0.30%$_{wt}$.

HYPSO-W1 [1/400] [1/400 dilution of radical to $Si(OEt)_4$]: Prepared analogously to **HYPSO-W1 [1/75]** using 638 mg of Pluronic® P-123, 26.4 mL of pH = 1.5 aqueous HCl, 1.67 mL (7.46 mmol) $Si(OEt)_4$, 19 mg (0.019 mmol) of radical **1**, and 12 mg (0.28 mmol) of NaF to afford 465 mg of **HYPSO-W1 [1/400]** as an off-white solid. IR (DRIFT): 3739 (m), 3522 (w, br), 2975 (w), 2937 (w), 2882 (w), 1870 (m, br), 1705 (s), 1692 (s) cm^{-1}. Elemental analysis: C = 3.08%$_{wt}$; H = 1.25%$_{wt}$; N =0.25%$_{wt}$.

Synthesis of HYPSO-W2 Materials:

HYPSO-W2 [100/1] [100/1 dilution of $Si(OEt)_4$ to $(EtO)_3SiCH_2CH_2Si(OEt)_3$ (**2**)]: Prepared analogously to **HYPSO-W1 [1/75]**, with **1**, $Si(OEt)_4$, and **2** mixed thoroughly before addition. Synthesized using 638 mg of Pluronic® P-123, 26.4 mL of pH = 1.5 aqueous HCl, 1.63 mL (7.30 mmol) of $Si(OEt)_4$, 27 μL (0.073 mmol) of $(EtO)_3SiCH_2CH_2Si(OEt)_3$ (**2**), 39 mg (0.038 mmol) of radical **1**, and 12 mg (0.28 mmol) NaF to afford 440 mg of **HYPSO-W2 [100/1]** as a pale yellow solid. IR (DRIFT): 3739 (w), 3410 (w, br), 2976 (w), 2938 (w), 2878 (w), 1865 (w, br), 1742 (m), 1704 (s), 1677(s) cm^{-1}. Elemental analysis: C = 7.60%$_{wt}$; H = 1.87%$_{wt}$; N =0.40%$_{wt}$.

HYPSO-W2 [50/1] [50/1 dilution of $Si(OEt)_4$ (**3a**) to $(EtO)_3SiCH_2CH_2Si(OEt)_3$ (**3b**)]: Prepared analogously to **HYPSO-W2 [100/1]** using 638 mg of Pluronic® P-123, 26.4 mL of pH = 1.5 aqueous HCl, 1.60 mL (7.17 mmol) of $Si(OEt)_4$, 52 μL (0.14 mmol) of $(EtO)_3SiCH_2CH_2Si(OEt)_3$ (**2**), 39 mg (0.038 mmol) of radical **1**, and 12 mg (0.28 mmol) NaF to afford 404 mg of **HYPSO-W2 [50/1]** as a pale yellow solid. IR (DRIFT): 3741 (m), 3521 (w, br), 2965 (w), 2941 (w), 2890 (w), 1871 (m, br), 1701 (s), 1683 (s) cm^{-1}. Elemental analysis: C = 3.72%$_{wt}$; H = 1.45%$_{wt}$; N =0.44%$_{wt}$.

HYPSO-W2 [25/1] [25/1 dilution of $Si(OEt)_4$ to $(EtO)_3SiCH_2CH_2Si(OEt)_3$ (**2**)]: Prepared analogously to **HYPSO-W2 [100/1]** using 638 mg of Pluronic® P-123, 26.4 mL of pH = 1.5 aqueous HCl, 1.54 mL (6.91 mmol) of $Si(OEt)_4$, 102 μL (0.276 mmol) of $(EtO)_3SiCH_2CH_2Si(OEt)_3$ (**2**), 39 mg (0.038 mmol) of radical **1**, and 12 mg (0.28 mmol) NaF to afford 430 mg of **HYPSO-W2 [25/1]** as a pale yellow solid. IR (DRIFT): 3738 (m), 3528 (w, br), 2968 (w), 2937 (w), 2897 (w), 1866 (m, br), 1743 (m), 1703 (s), 1692 (s) cm^{-1}. Elemental analysis: C = 4.52%$_{wt}$; H = 1.49%$_{wt}$; N =0.39%$_{wt}$.

HYPSO-W2 [2/1] [2/1 dilution of $Si(OEt)_4$ to $(EtO)_3SiCH_2CH_2Si(OEt)_3$ (**2**)]: Prepared analogously to **HYPSO-W2 [100/1]** using 638 mg of Pluronic® P-123, 26.4 mL of pH = 1.5 aqueous HCl, 833 μL (3.73 mmol) of $Si(OEt)_4$, 692 μL (1.87 mmol) of $(EtO)_3SiCH_2CH_2Si(OEt)_3$ (**2**), 39 mg (0.038 mmol) of radical **1**, and 12 mg (0.28 mmol) NaF to afford 476 mg of **HYPSO-W2 [2/1]** as a pale

yellow solid. IR (DRIFT): 3730 (m), 3472 (m, br), 2966 (w), 2893 (m), 2810 (w), 1739 (m), 1701 (s), cm^{-1}. Elemental analysis: C = 11.53%$_{wt}$; H = 2.67%$_{wt}$; N =0.40%$_{wt}$.

Table S1. Nitrogen adsorption properties of **HYPSO-W1** and **HYPSO-W2**

material (dilution)	surface area (m^2/g)[a]	pore volume (cm^3/g)[b]	peak pore diameter (nm)[b]
HYPSO-W1 [1/75]	673	1.1	8.1
HYPSO-W1 [1/100]	807	1.0	8.1
HYPSO-W1 [1/200]	789	1.2	9.2
HYPSO-W1 [1/300]	935	1.2	8.1
HYPSO-W1 [1/400]	987	1.2	8.1
HYPSO-W2 [100/1]	690	1.0	8.1
HYPSO-W2 [50/1]	904	0.8	8.1
HYPSO-W2 [25/1]	1066	1.1	9.2
HYPSO-W2 [2/1]	851	0.7	5.4

All materials display typical Type IV isotherms. [a] Calculated using Brunauer-Emmet-Teller (BET) analysis.
[b] Calculated using Barrett-Joyner-Halenda (BJH) analysis.

Table S2. SA-XRD properties of **HYPSO-W1** and **HYPSO-W2**

material (dilution)	structure[a]	d(100) [nm]	A0 (nm)[b]	wall thickness (nm)[c]
HYPSO-W1 [1/75]	hexagonal	10.8	12.4	4.3
HYPSO-W1 [1/100]	hexagonal	10.6	12.3	4.2
HYPSO-W1 [1/200]	hexagonal	11.0	12.7	3.5
HYPSO-W1 [1/300]	hexagonal	10.5	12.1	4.0
HYPSO-W1 [1/400]	hexagonal	10.4	12.0	3.9
HYPSO-W2 [100/1]	hexagonal	10.5	12.1	4.0
HYPSO-W2 [50/1]	hexagonal	10.4	12.0	3.9
HYPSO-W2 [25/1]	hexagonal	10.4	12.0	2.8
HYPSO-W2 [2/1]	wormlike	9.7	11.2	5.8

[a] Determined by analysis of SA-XRD lineshape. [b] Calculated by $2*d(100)/3^{(1/2)}$ based on a hexagonal unit cell.
[c]Calculated by A0-peak pore diameter

N_2 Adsorption/Desorption Isotherm of **HYPSO-W1 [1/75]**

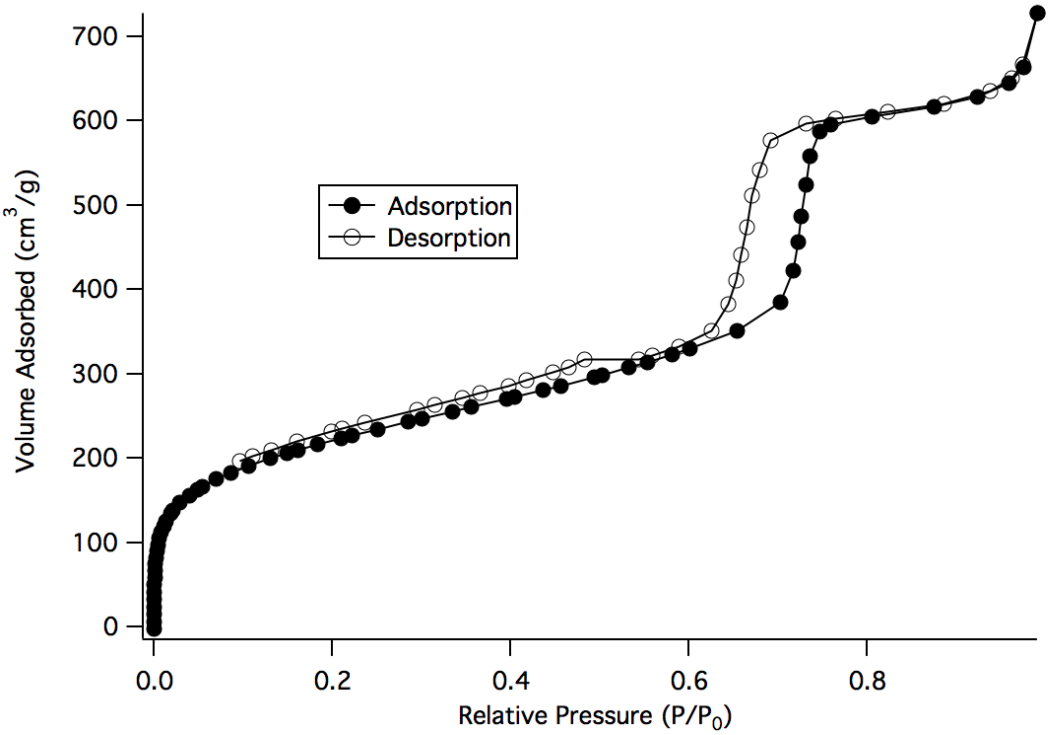

N_2 Adsorption/Desorption Isotherm of **HYPSO-W1 [1/100]**

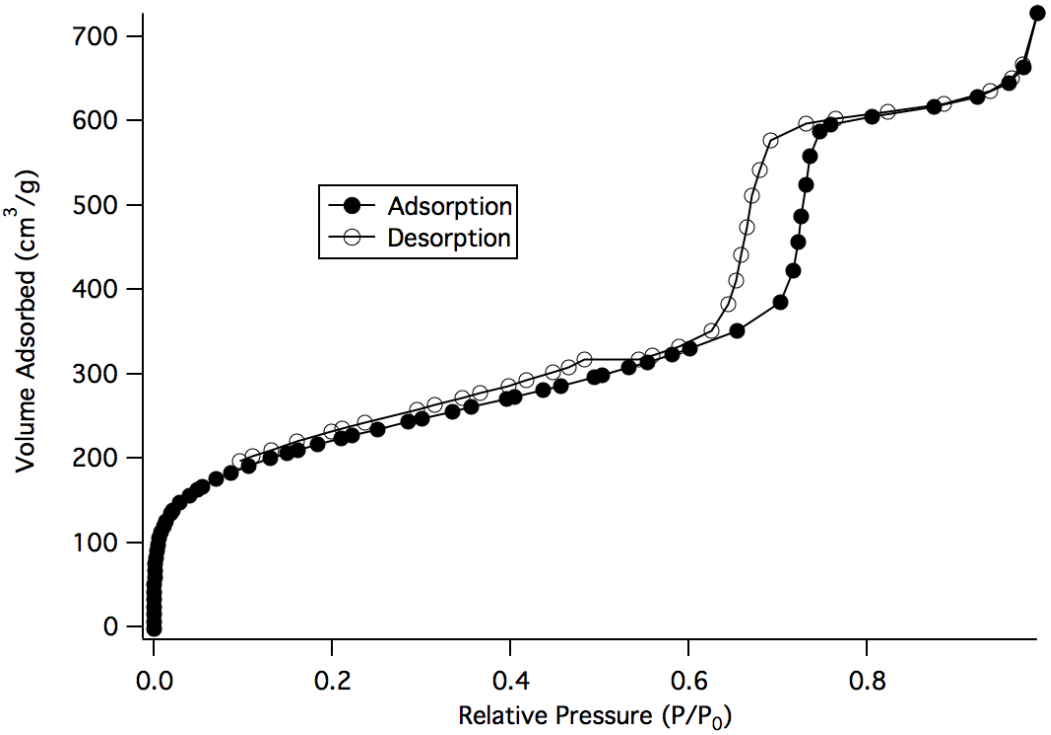

N_2 Adsorption/Desorption Isotherm of **HYPSO-W1 [1/200]**

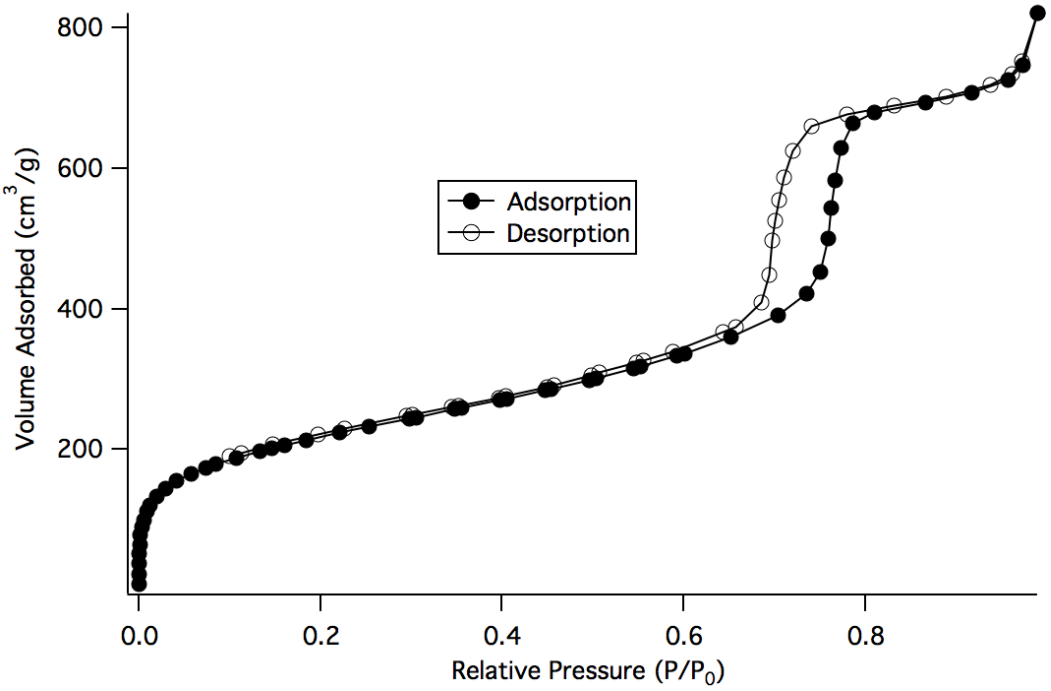

N_2 Adsorption/Desorption Isotherm of **HYPSO-W1 [1/300]**

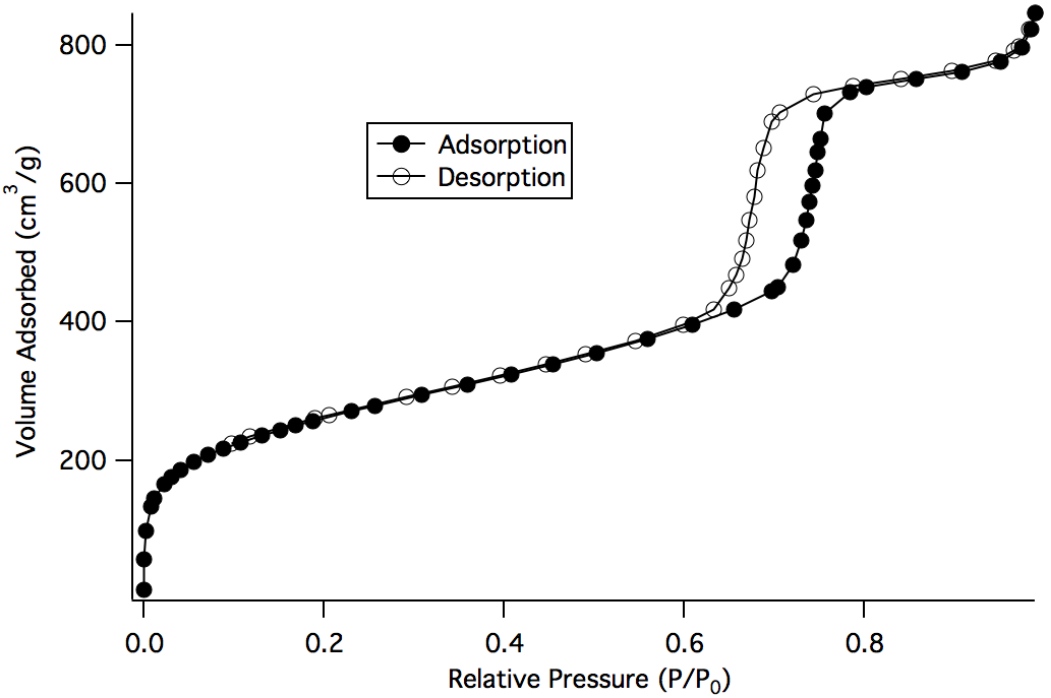

N_2 Adsorption/Desorption Isotherm of **HYPSO-W1 [1/400]**

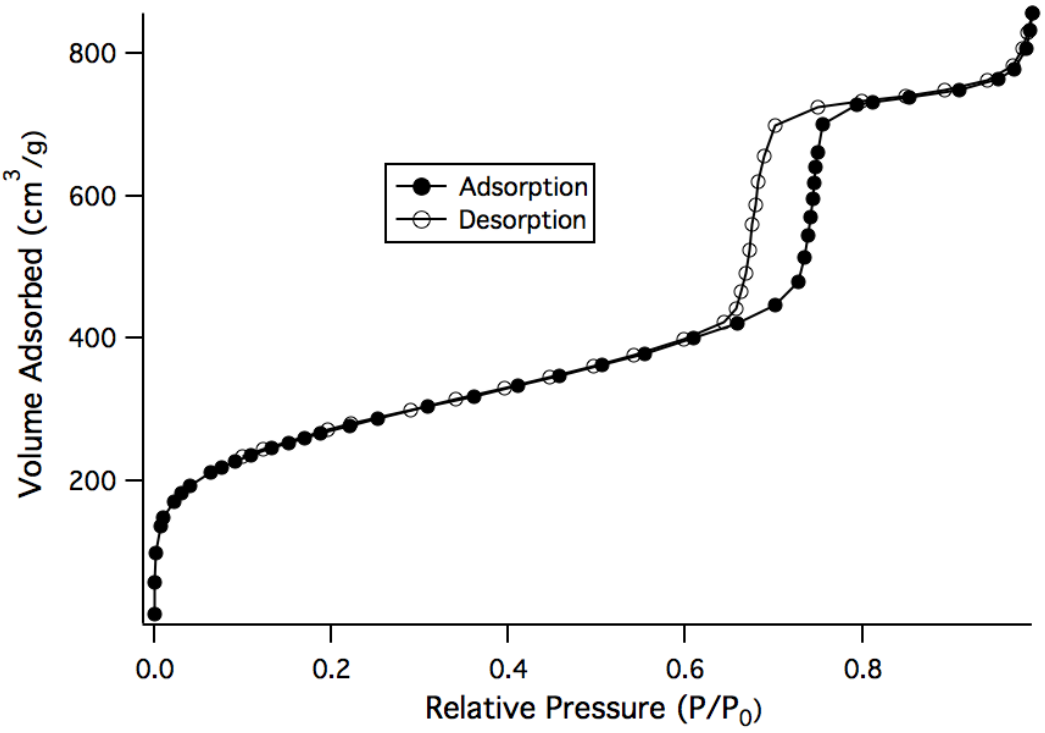

N_2 Adsorption/Desorption Isotherm of **HYPSO-W2 [100/1]**

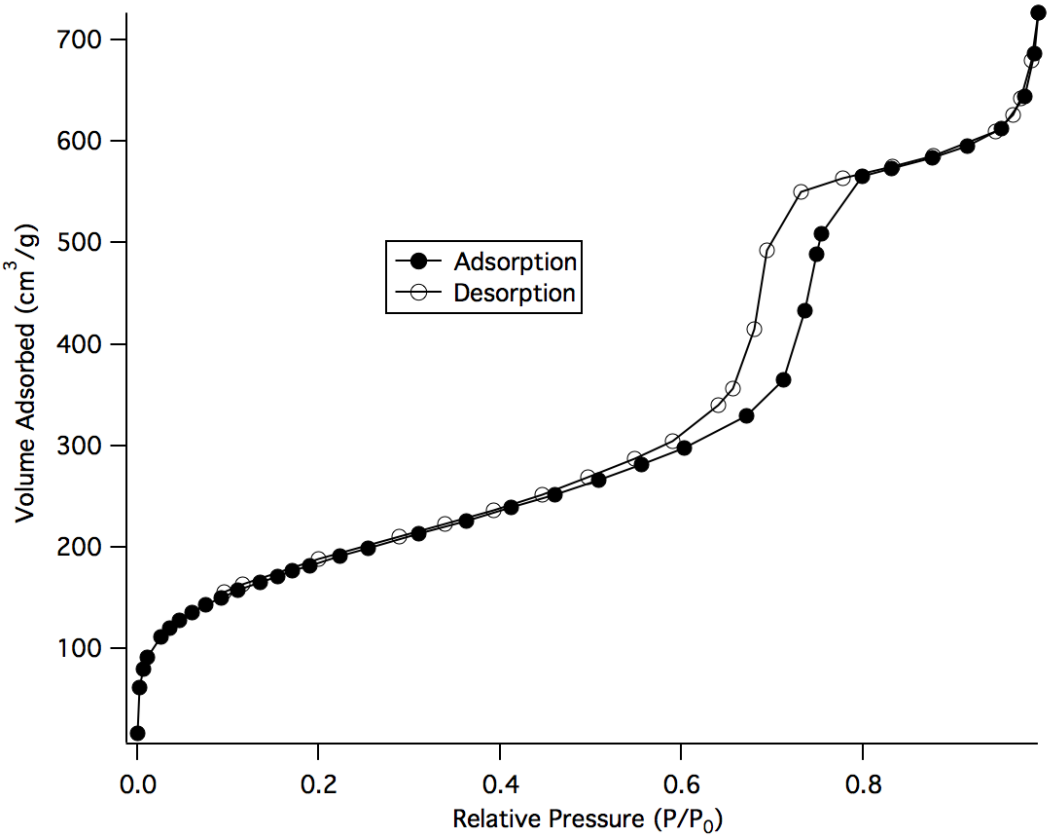

N_2 Adsorption/Desorption Isotherm of **HYPSO-W2 [50/1]**

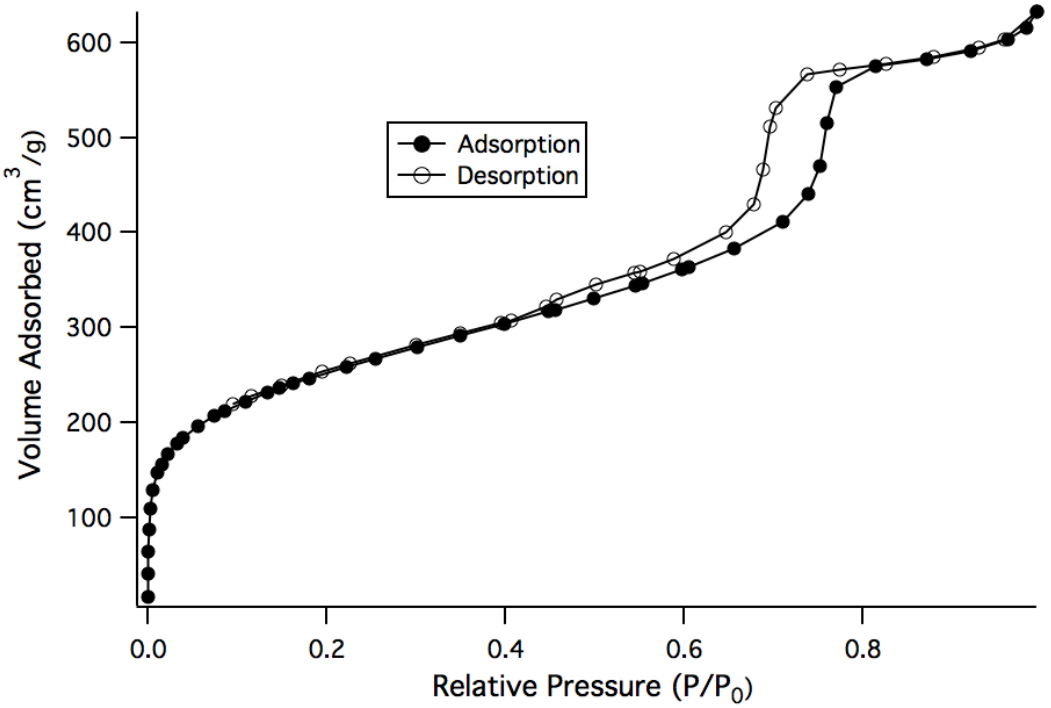

N_2 Adsorption/Desorption Isotherm of **HYPSO-W2 [25/1]**

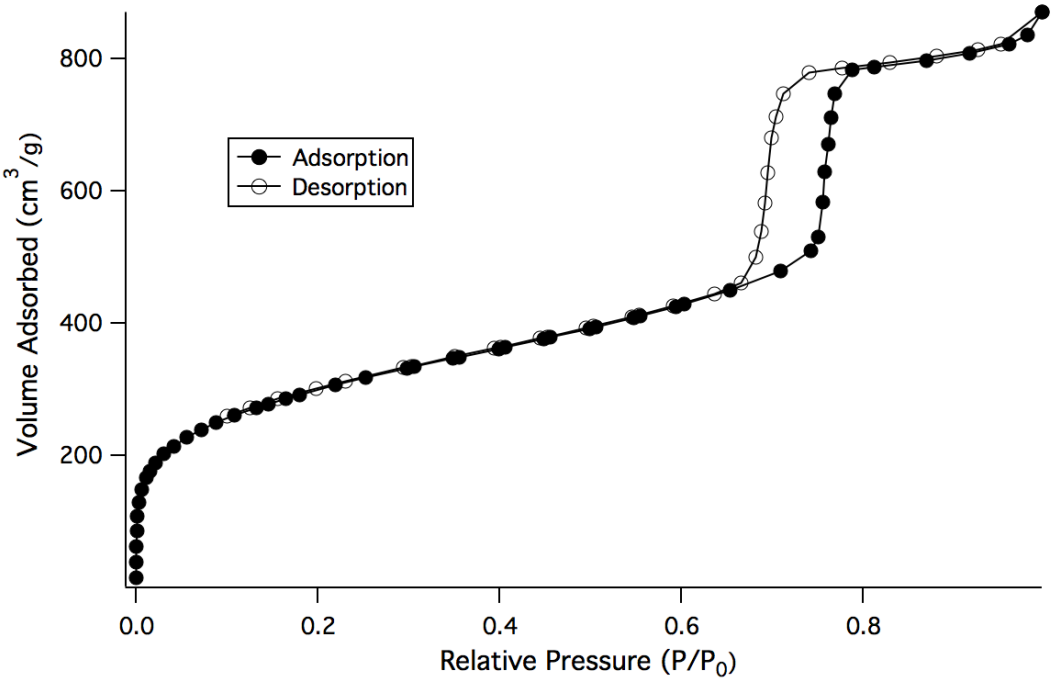

N_2 Adsorption/Desorption Isotherm of **HYPSO-W2 [2/1]**

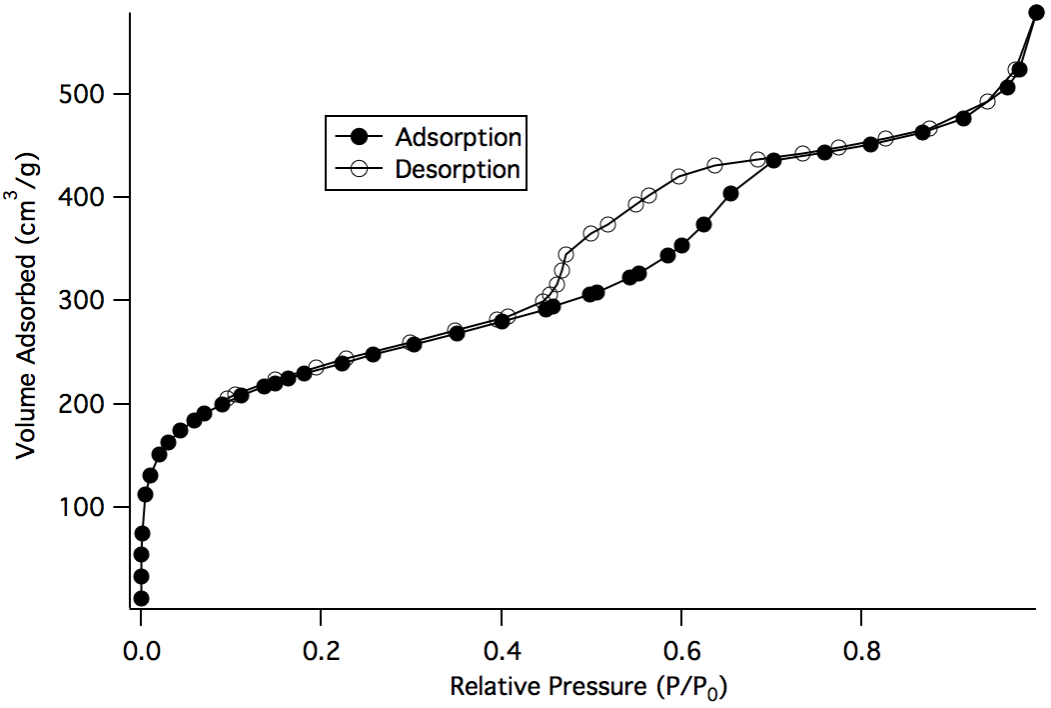

X-Ray Diffraction (XRD) Pattern of **HYPSO-W1 [1/75]**

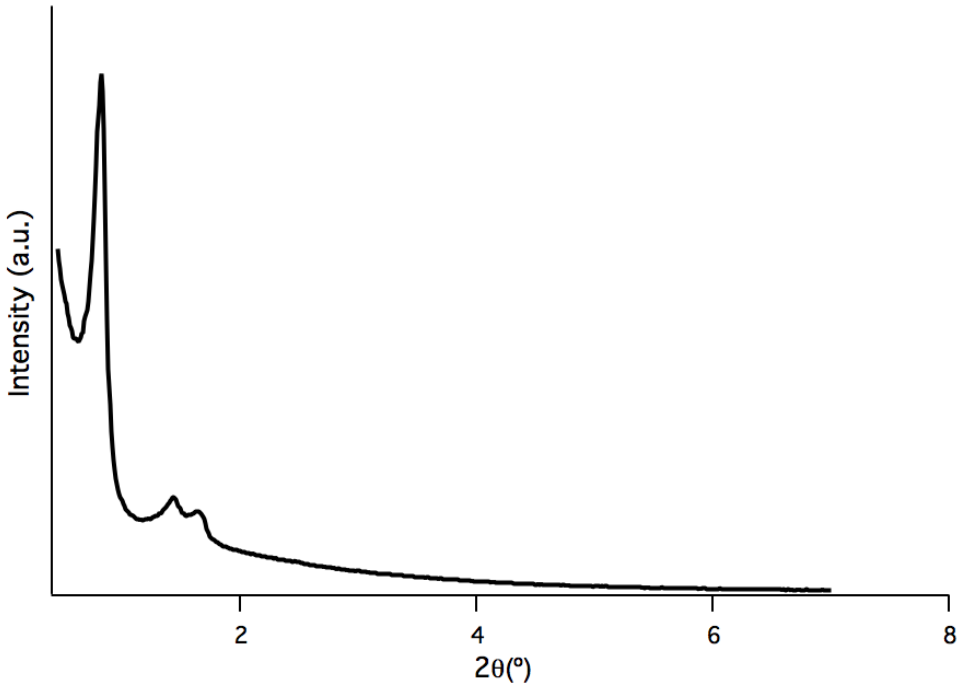

X-Ray Diffraction (XRD) Pattern of **HYPSO-W1 [1/100]**

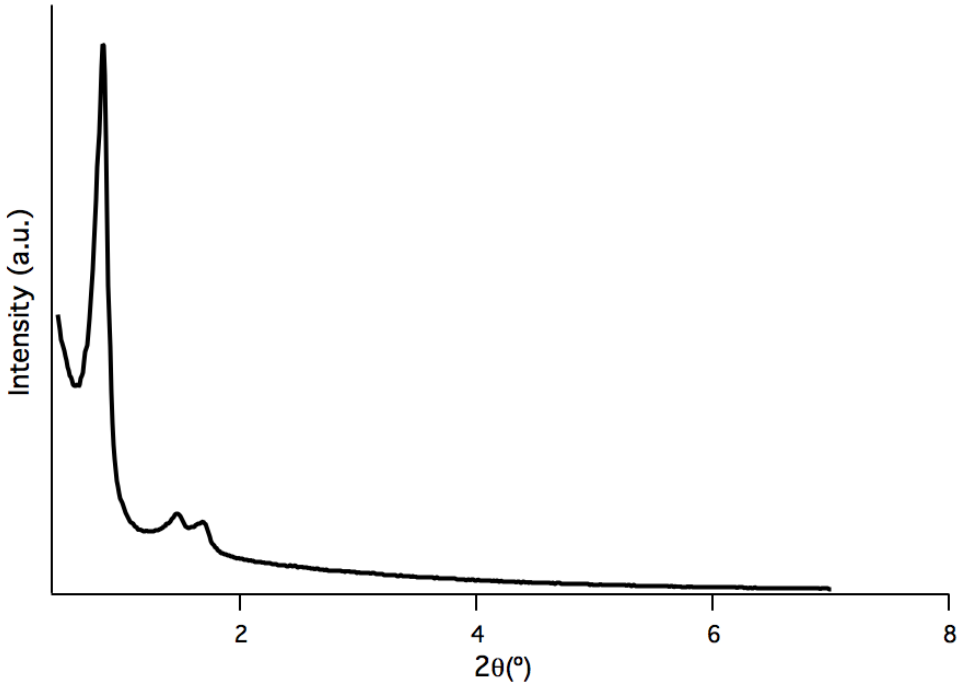

X-Ray Diffraction (XRD) Pattern of **HYPSO-W1 [1/200]**

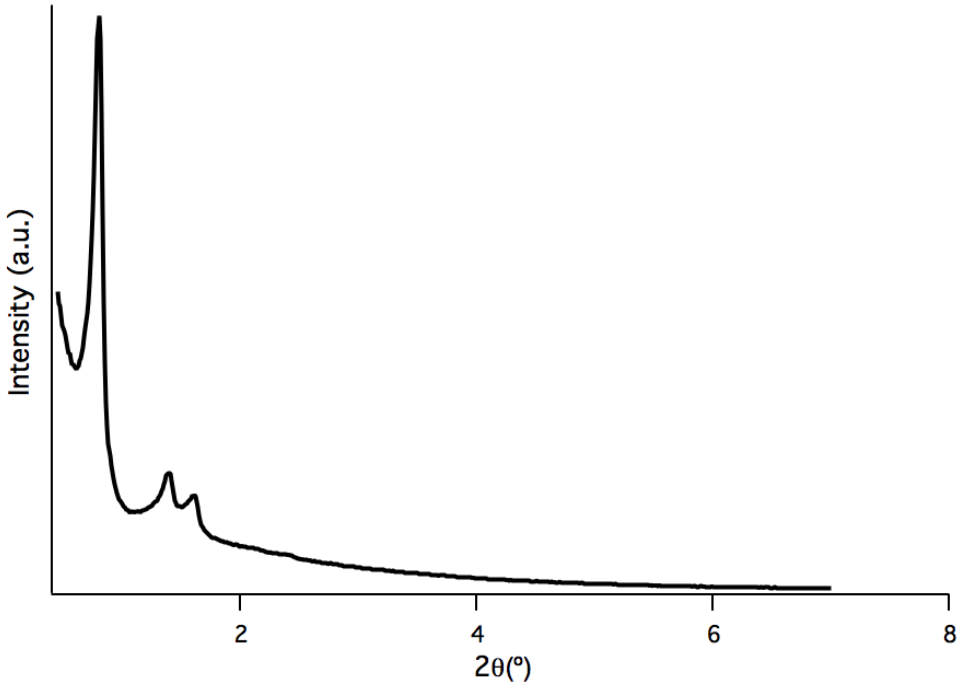

X-Ray Diffraction (XRD) Pattern of **HYPSO-W1 [1/300]**

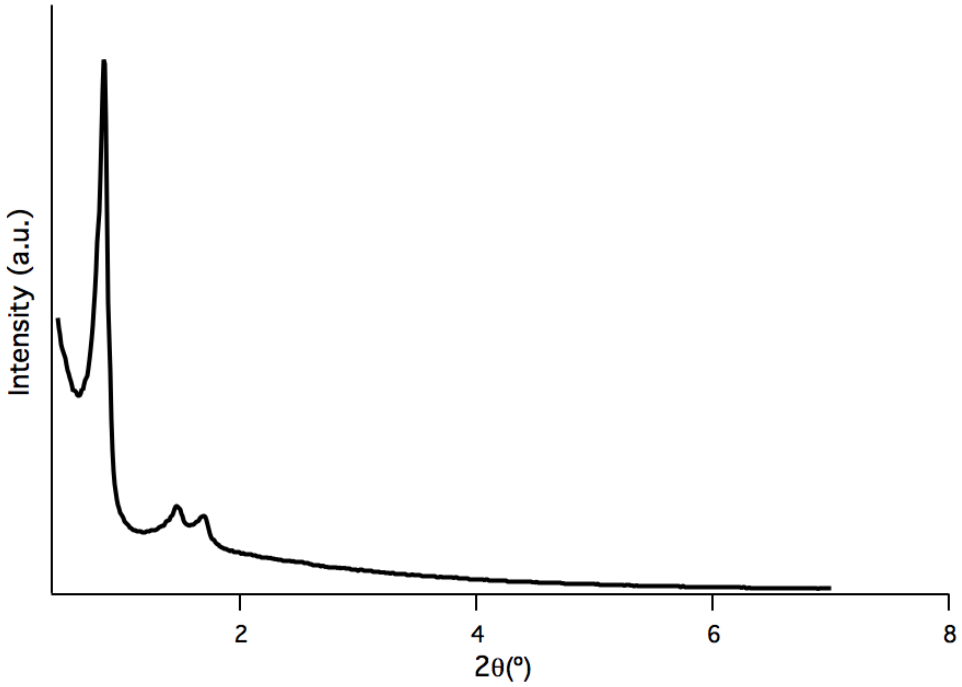

X-Ray Diffraction (XRD) Pattern of **HYPSO-W1 [1/400]**

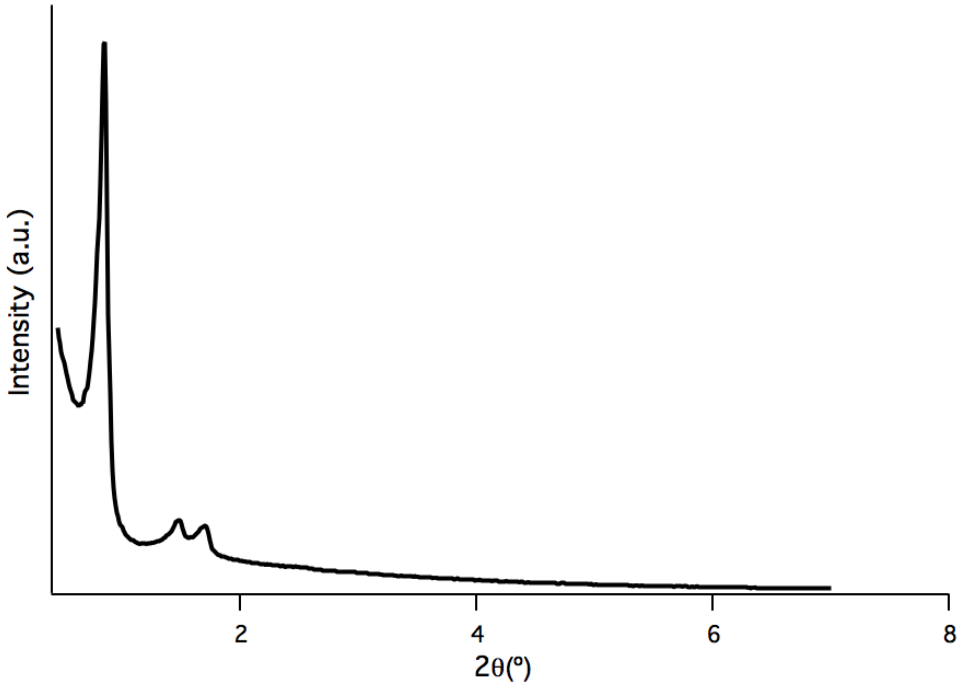

X-Ray Diffraction (XRD) Pattern of **HYPSO-W2 [100/1]**

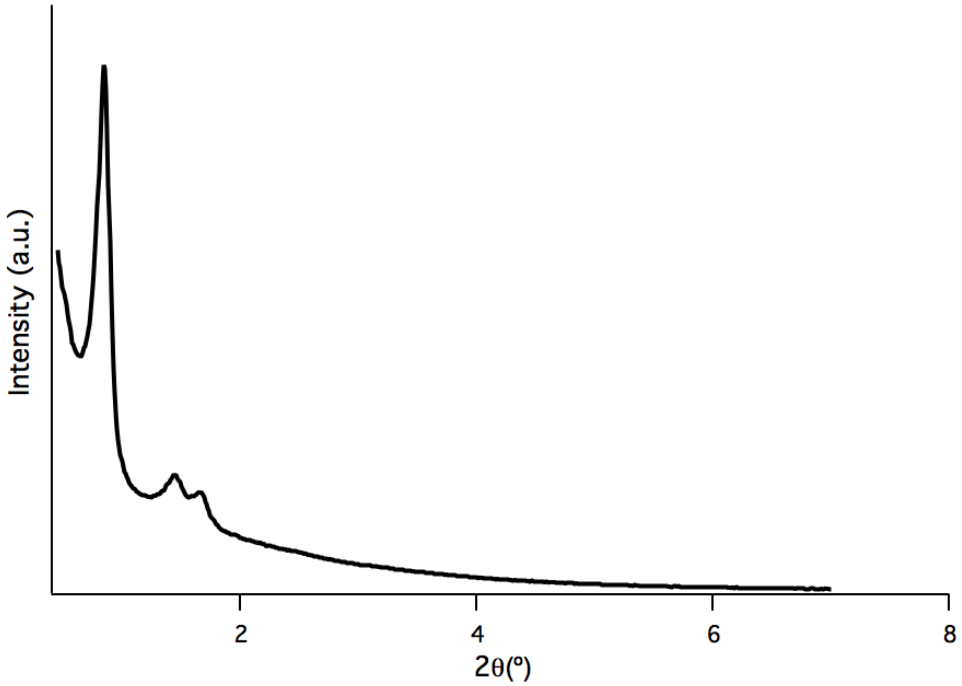

X-Ray Diffraction (XRD) Pattern of **HYPSO-W2 [50/1]**

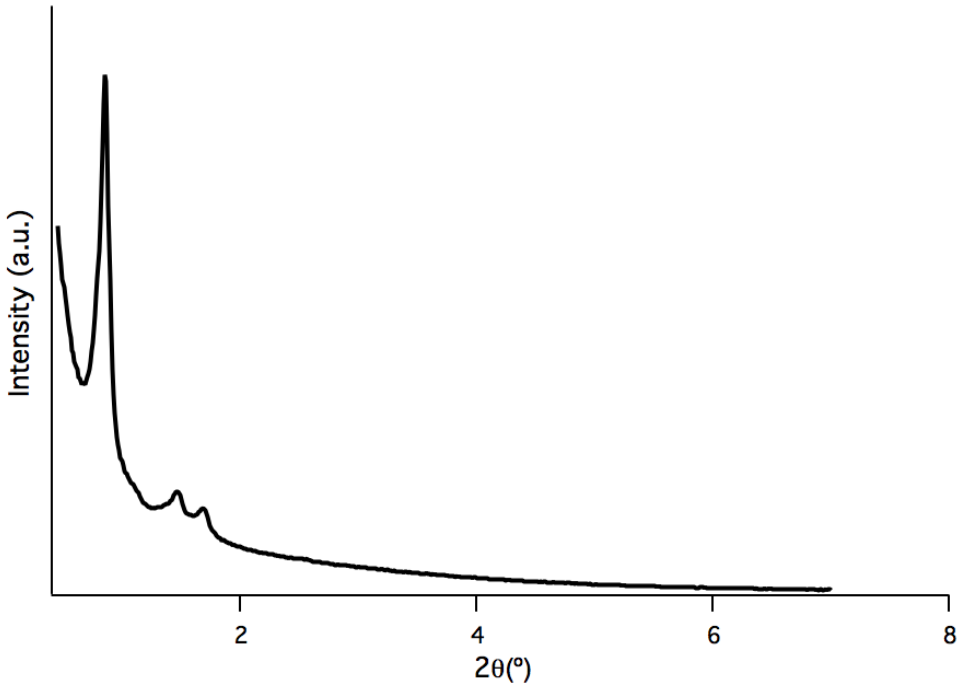

X-Ray Diffraction (XRD) Pattern of **HYPSO-W2 [25/1]**

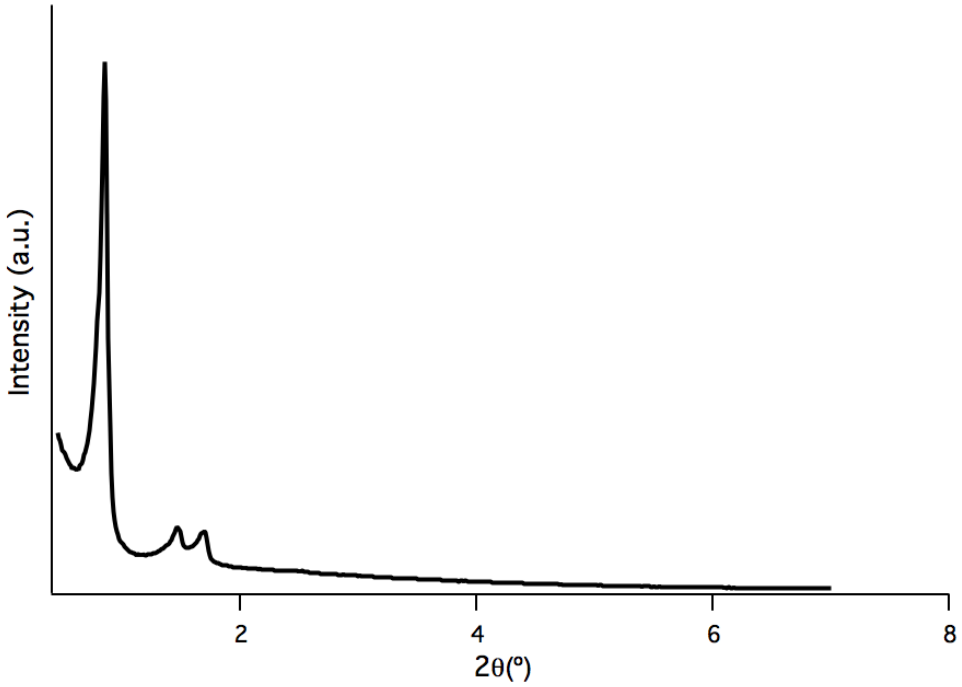

X-Ray Diffraction (XRD) Pattern of **HYPSO-W2 [2/1]**

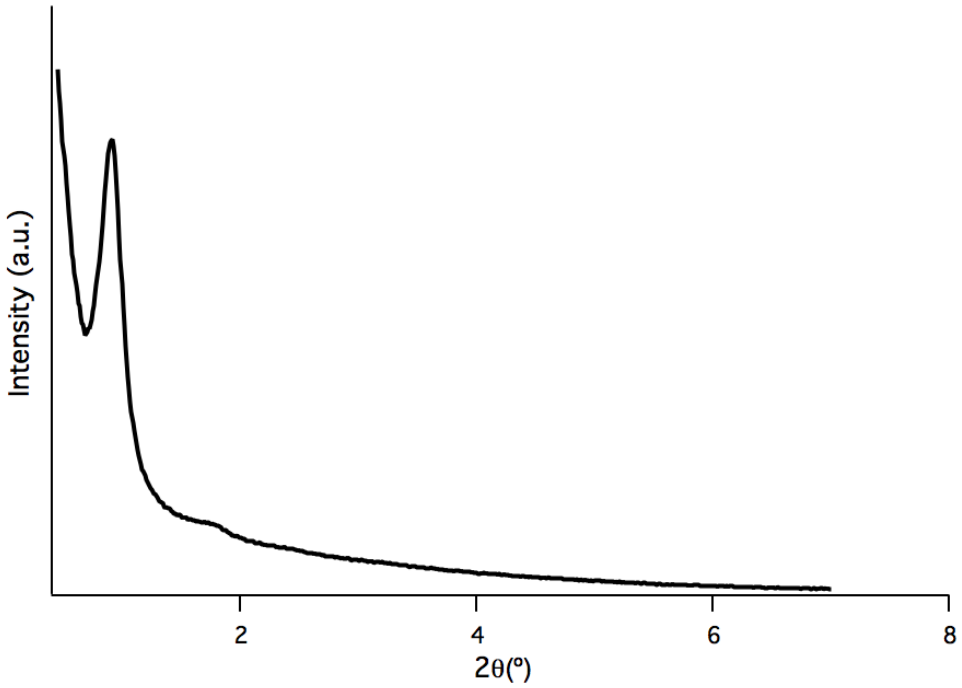

Table S3. EPR properties of **HYPSO-W1** and **HYPSO-W2**

material (dilution)	radical conc. (mmol/g)[a]	linewidth (Gauss)[b]	T_{1e}^{*}[μs] (β)[c]	T_{2e}^{*}[ns][d]	$<T_{1e}>$ [μs][e]
HYPSO-W1 [1/75]	0.11	13.1	18 (0.53)	157	32
HYPSO-W1 [1/100]	0.088	13.0	22 (0.53)	179	39
HYPSO-W1 [1/200]	0.045	12.5	69 (0.65)	364	95
HYPSO-W1 [1/300]	0.026	12.3	117 (0.72)	495	145
HYPSO-W1 [1/400]	0.022	12.3	177 (0.75)	638	210
HYPSO-W2 [100/1]	0.045	12.1	64 (0.68)	303	84
HYPSO-W2 [50/1]	0.042	12.1	68 (0.67)	290	90
HYPSO-W2 [25/1]	0.033	12.1	102 (0.71)	403	128
HYPSO-W2 [2/1]	0.040	11.7	69 (0.67)	311	91

[a] Determined by CW EPR spectroscopy. [b] Taken at ~110 K using CW EPR spectroscopy with samples incipient wetness impregnated (IWI) with 1,1,2,2-tetrachloroethane (TCE). [c]Determined from an inversion recovery experiment in pulsed EPR at ~105 K with samples IWI with TCE. The data were fitted using a stretched exponential function. [d] Determined from an inversion recovery experiment in pulsed EPR at ~105 K with samples IWI with TCE. The data were fitted using a mono-exponential decay function. [e]Mean relaxation time.

Ascorbic Acid Treatment of Materials: Materials (20.0–100 mg) were weighed into a watch glass and impregnated by incipient wetness impregnation[4] using a freshly prepared 0.2 M solution of aqueous ascorbic acid. A volume equal to 3.5 times the pore volume of the material (at least 10 equiv. based on the radical concentration of the material) and was added in three portions and mixed with a glass stirring rod between additions. The wet material was allowed to stand at 23 ºC for two hours, after which time it was transferred to a porosity 3 fritted funnel and washed with deionized water (3 x 5 mL), acetone (3 x 5 mL), and pentanes (3 x 5 mL). To remove the excess ascorbic acid, the solid is then transferred to a 10 mL round bottomed flask containing a stir bar as well as a premixed solution of pyridine (1 mL), deionized water (1 mL), and a 2 M aqueous solution of HCl (0.33 mL). The reaction vessel is capped with a rubber septum containing a vent needle and allowed to stir at 65 ºC for 18 h. After allowing the vessel to cool to room temperature, the solid is collected on a porosity 3 glass-fritted funnel and washed with deionized water (3 x 5 mL), acetone (3 x 5 ml), and pentanes (3 x 5 mL). The solid is then dried for 12 hours under vacuum (10^{-4} Torr) at 135 ºC using a temperature ramp of 1 ºC/min from room temperature (~23 ºC).

Figure S1a. EPR spectra showing that **HYPSO-W1 [1/200]** is not especially vulnerable to ascorbic acid.

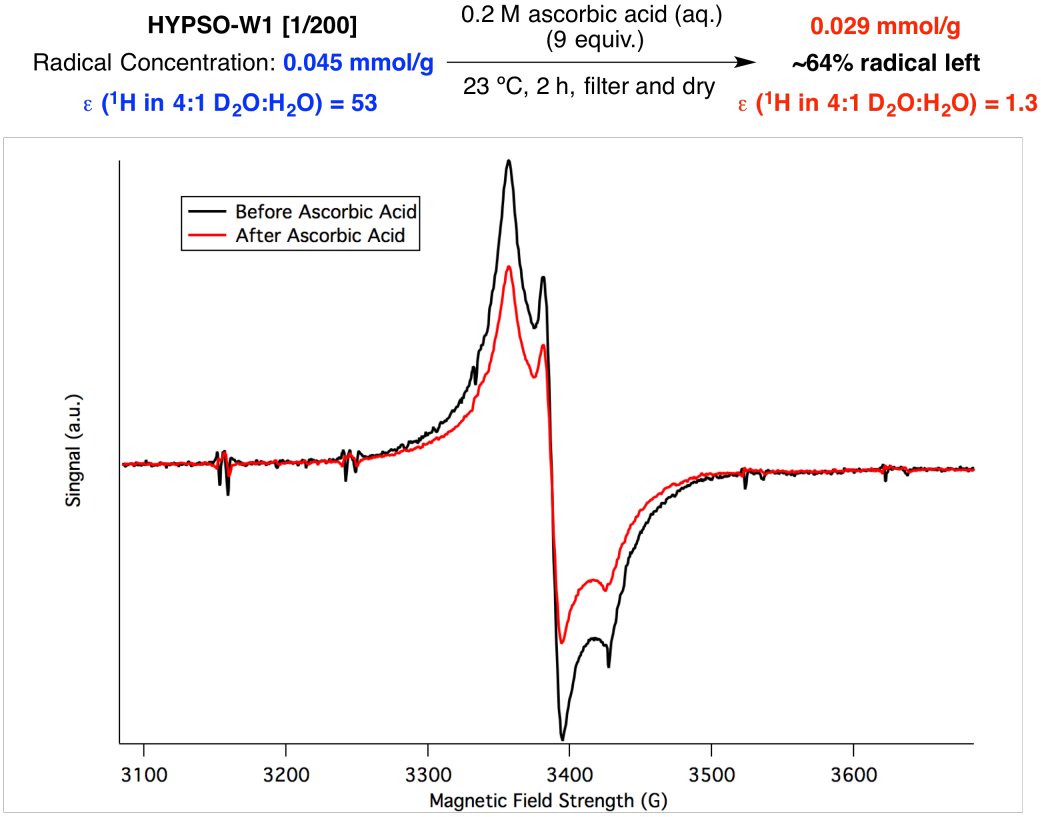

Continuous wave EPR spectra of **HYPSO-W1 [1/200]** material before and after ascorbic acid treatment, showing radicals in the wall are more resistant to decomposition than those in the pores. However, this treated material shows little to no DNP effect at 600 MHz (14.1 T) and ~100 K with 10 kHz MAS with 4:1 ratio of D_2O:H_2O as a solvent.

Figure S1b. EPR spectra showing complete decomposition of radicals in **HYPSO-1** material.

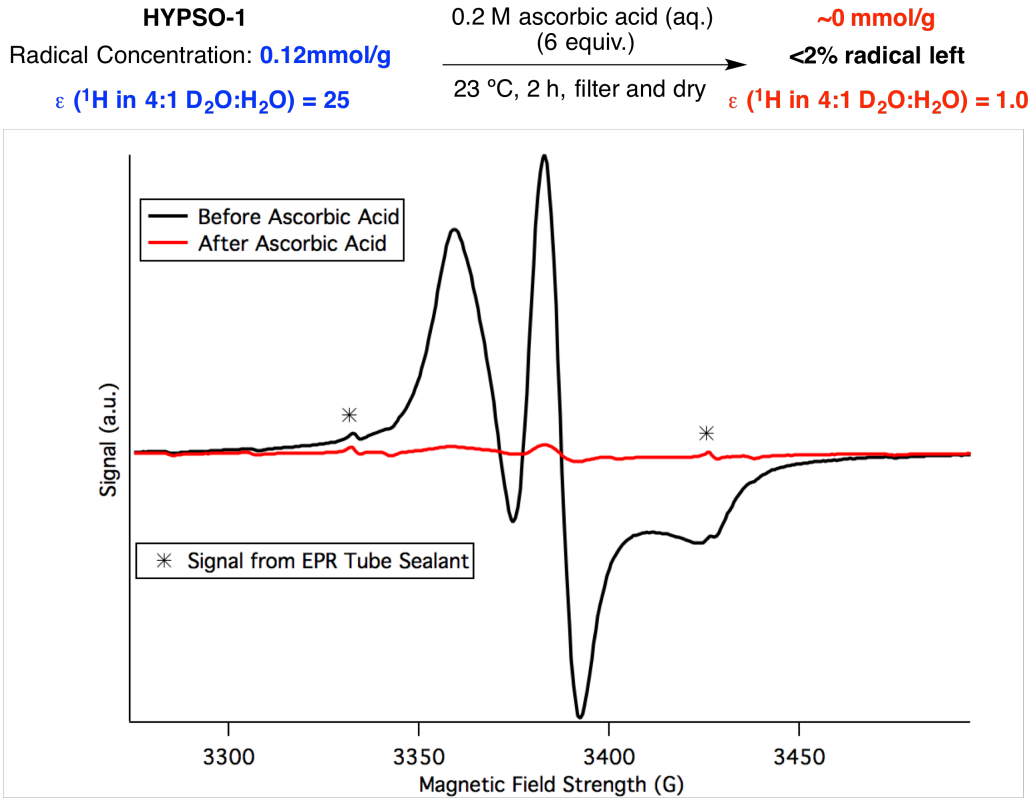

Continuous wave EPR spectra of HYPSO-1 material before and after ascorbic acid treatment, showing the radicals localized in the pores of the material are very vulnerable to decomposition. DNP enhancement measured at 600 MHz (14.1 T) and ~100 K with 10 kHz MAS.

DNP Enhancement of Different Radical Solutions in SBA-15

Table S4. DNP enhancement of different radical solutions in SBA-15

entry	***Solvent***	radical	^{1}H enhancement (ε)[a]	T_1(s)[b]
1	4:1 D_2O:H_2O	AMUPol	51	60
2	$C_2H_2Cl_4$ (TCE)	TEKPol	35	5
3	4:1 D18-decalin:decalin[c]	TEKPol	2	n.d.
4	4:1 D8-toluene:D3-toluene	TEKPol	8[d]	7
5	H3-formamide	AMUPol	85	24
6	D6-DMSO	AMUPol	18	5

[a]Enhancements determined at 600 MHz proton frequency (14.1 T) and ~100 K with 10 kHz MAS. [b]Determined by a saturation recovery experiment. [c]Both TEKPol and AMUPol were completely insoluble in decalin. [d]Enhancement of ^{13}C nucleus instead of ^{1}H due to sample melting under even the lowest μW power.

For a solution of a polarizing agent (AMUPol) in 4:1 D_2O:H_2O added to mesoporous silica (SBA-15; surface area 944 m^2/g, pore volume 1.5 cm^3/g, pore diameter 9.2 nm) that does not contain any radical, we obtain an enhancement of 51 (at 14.1 T), similar to that obtained with the **HYPSO-W1 [1/200]** material. On the contrary, when this experiment is carried out with TEKPol in 4:1 D18:H18 decalin as the solvent, an enhancement of only 2 is obtained (vs. 15 for the **HYPSO-W1 [1/200]** material under the same conditions), likely due to the aforementioned insolubility of the radicals in this solvent (see Table S4).

Table S5. Synthesis of materials containing radicals in the walls with and without organic dopant **2** and their performance in MAS DNP-Companion table to Figure 2.

entry	material [dilution]	radical conc. (mmol/g)[yield][a]	^{1}H enhancement (ε)[b]	T_1 (s)[c]
	HYPSO-W1 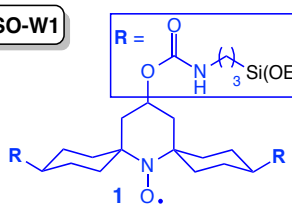 1) ***X* equiv. Si(OEt)$_4$**, Pluronic 123®, 0.032 M HCl (aq.), 45 °C, NaF, 18 h → 2) 3:3:1 pyridine:H_2O:2M HCl, 65 °C, 18 h 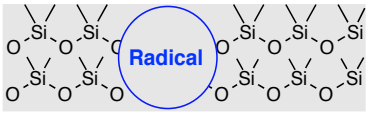 **Radical** in **Walls** Material **HYPSO-W1** **[1/X] = Radical 1/Si(OEt)$_4$**			
1	**HYPSO-W1 [1/75] [1/Si(OEt)$_4$]**	0.11[56%]	56	28
2	**HYPSO-W1 [1/100]**	0.087[58%]	51	32
3	**HYPSO-W1 [1/200]**	0.045[58%]	53	39
4	**HYPSO-W1 [1/300]**	0.026[49%]	34	69
5	**HYPSO-W1 [1/400]**	0.022[54%]	22	61
	HYPSO-W2 **Radical 1** + X Si(OEt)$_4$ + (EtO)$_3$Si 2 Si(OEt)$_3$ → 1)Pluronic 123®, 0.032 M HCl, 45 °C, NaF, 18 h → 2) 3:3:1 pyridine:H_2O:2M HCl, 65 °C, 18 h 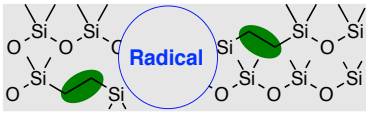 **Organic**-doped **HYPSO-W2** **[X/1] = Si(OEt)$_4$/Dopant 2** **Radical 1/Σsilicon** = 1/200			
6	**HYPSO-W2 [100/1] [Si(OEt)$_4$/2]**	0.045[57%]	42	53
7	**HYPSO-W2 [50/1]**	0.042[54%]	45	43
8	**HYPSO-W2 [25/1]**	0.033[43%]	32	82
9	**HYPSO-W2 [2/1]**	0.040[57%]	43	44

(a) Determined by continuous wave (CW) EPR spectroscopy. (b) Enhancements determined at 600 MHz proton frequency (14.1 T) and ~100 K with 10 kHz MAS with 4:1 D_2O:H_2O as a solvent. (c) Determined by a saturation recovery experiment.

Table S6. DNP enhancements (ε) obtained using HYPSO-W2 after treating the material with ascorbic acid-Companion table to Figure 2c.

HYPSO-W2 (Table 1b) → 0.2 M ascorbic acid (aq.) (13–23 equiv.), 23 °C, 2 h, filter and dry → Ascorbic acid-treated material

entry	material [ratio **2a/2b**]	radical conc. (mmol/g)[a] [% lost]	^{1}H enhancement (ε)[b]	% drop in ε
1	**HYPSO-W2** [100/1]	0.035[22%]	27	36
2	**HYPSO-W2** [50/1]	0.036[14%]	28	38
3	**HYPSO-W2** [25/1]	0.038 [0%]	32	0
4	**HYPSO-W2** [2/1]	0.033[17%]	39	9

(a) – (b) As in Table S5.

Table S7. MAS-DNP enhancements (ε) in various solvents and at various magnetic field strengths with **HYPSO-W1 [1/200]** - Companion table to Figure 3.

entry	***Solvent***	magnetic field (T)	^{1}H enhancement (ε)[a] / T_1 (s)[b]
1	4:1 D_2O:H_2O	14.1	53 / 44
2	$C_2H_2Cl_4$ (TCE)	14.1	14 / 15
3	4:1 D18-decalin:decalin	14.1	15 / 31
4	4:1 D8-toluene:D3-toluene	14.1	12[c] / 34
5	H3-formamide	14.1	37 / 31
6	D6-DMSO	14.1	15 / 5
7	9:1 D_2O:H_2O[d]	9.4	100 / 48
8	4:1 D_2O:H_2O	18.8	20 / n.d.

(a) Determined at given magnetic field at ~100 K. (b) Determined by a saturation recovery experiment. (c) Three times the amount of solvent used for IWI to prevent melting of sample. (d) 4:1 D_2O to H_2O gave a lower ^{1}H enhancement of 71 in this case, although there was no difference in enhancement between these two solvent ratios at 14.1 T. n.d.=not determined.

Field Profile of HYPSO-W1 [1/200] in a 600 MHz Spectrometer: DNP enhancement field profile was measured by altering the main magnetic field through increasing or decreasing the current in the sweep coil at 0.5 A increment. The ^{1}H NMR signal was used to track the change in field strength, which was allowed to stabilize for several minutes after each increment before the next measurement. The sample was prepared analogously to samples for MAS-DNP enhancement measurements with 4:1 D_2O:H_2O as the solvent.

Field Profile of **HYPSO-W1 [1/200]** in a 600 MHz Spectrometer

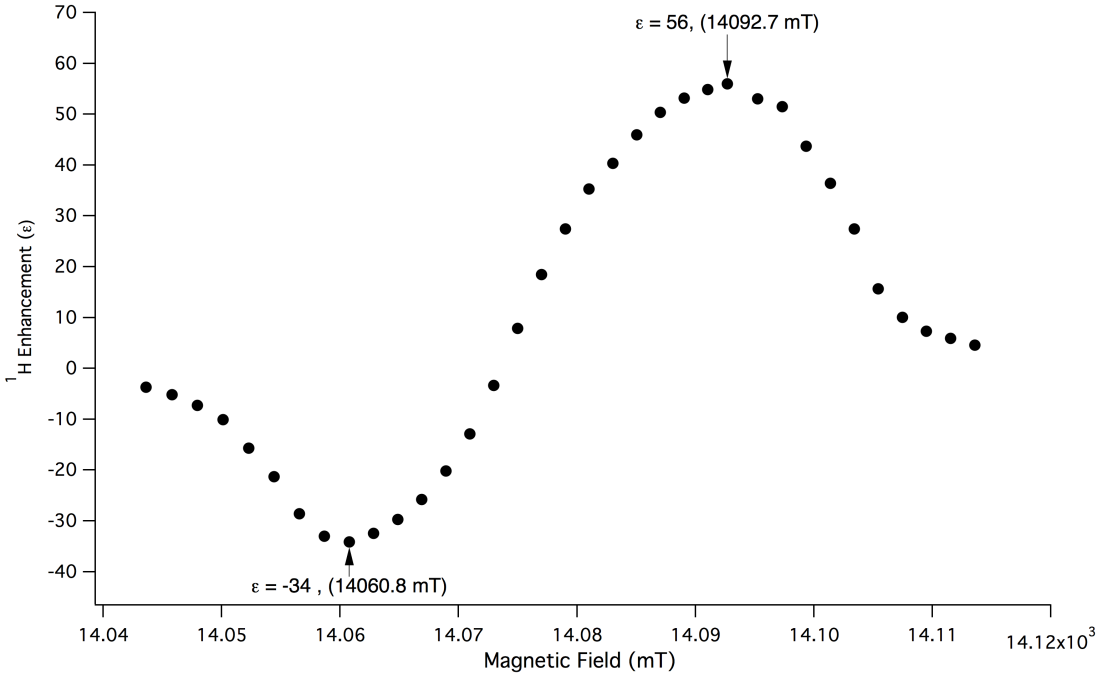

Field Profile of **HYPSO-W1 [1/200]** in 400 MHz Spectrometer

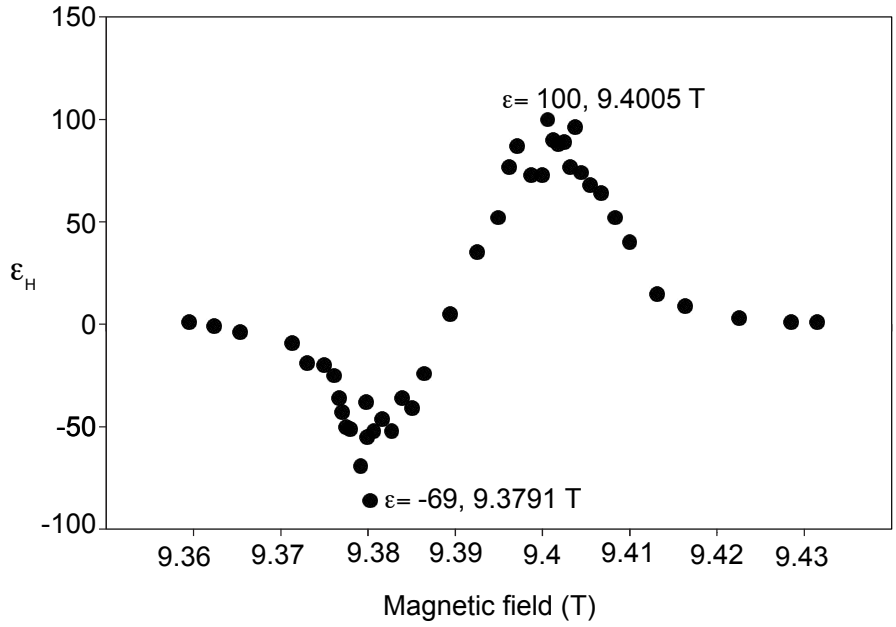

TEM Image of HYPSO-W1 [1/400]

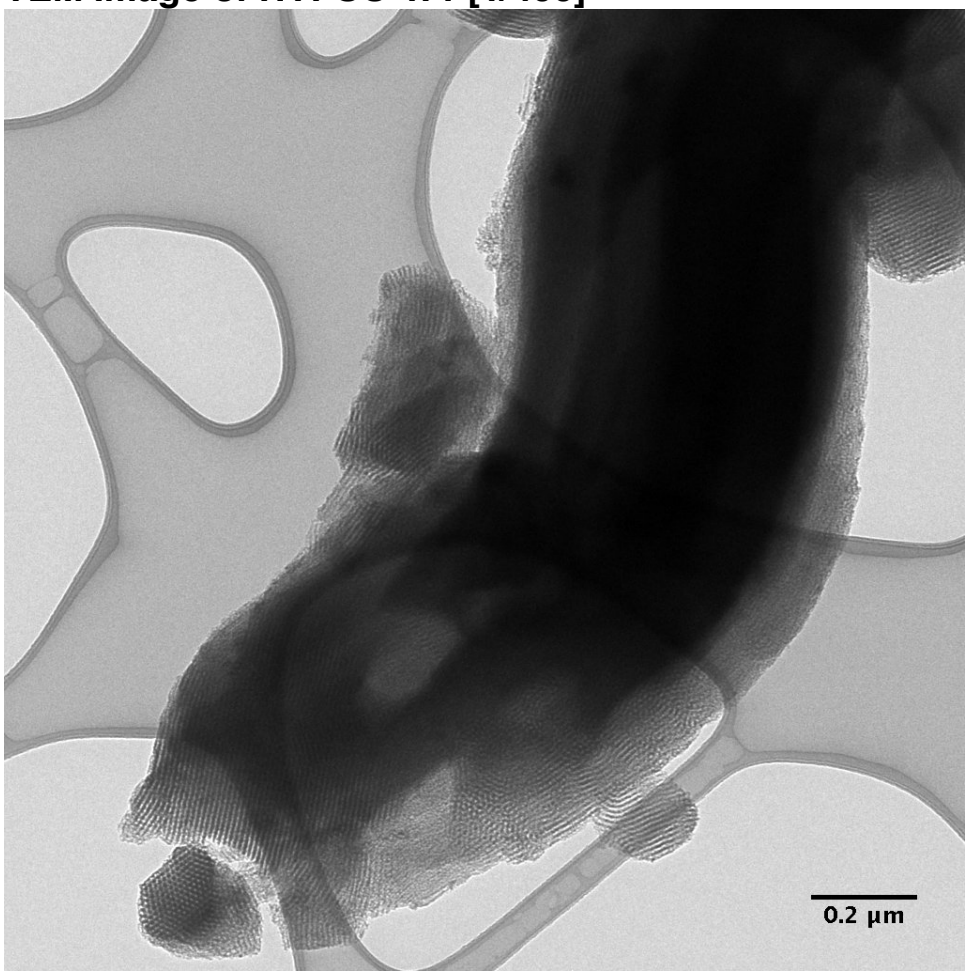

TEM Image of HYPSO-W2 [50/1]

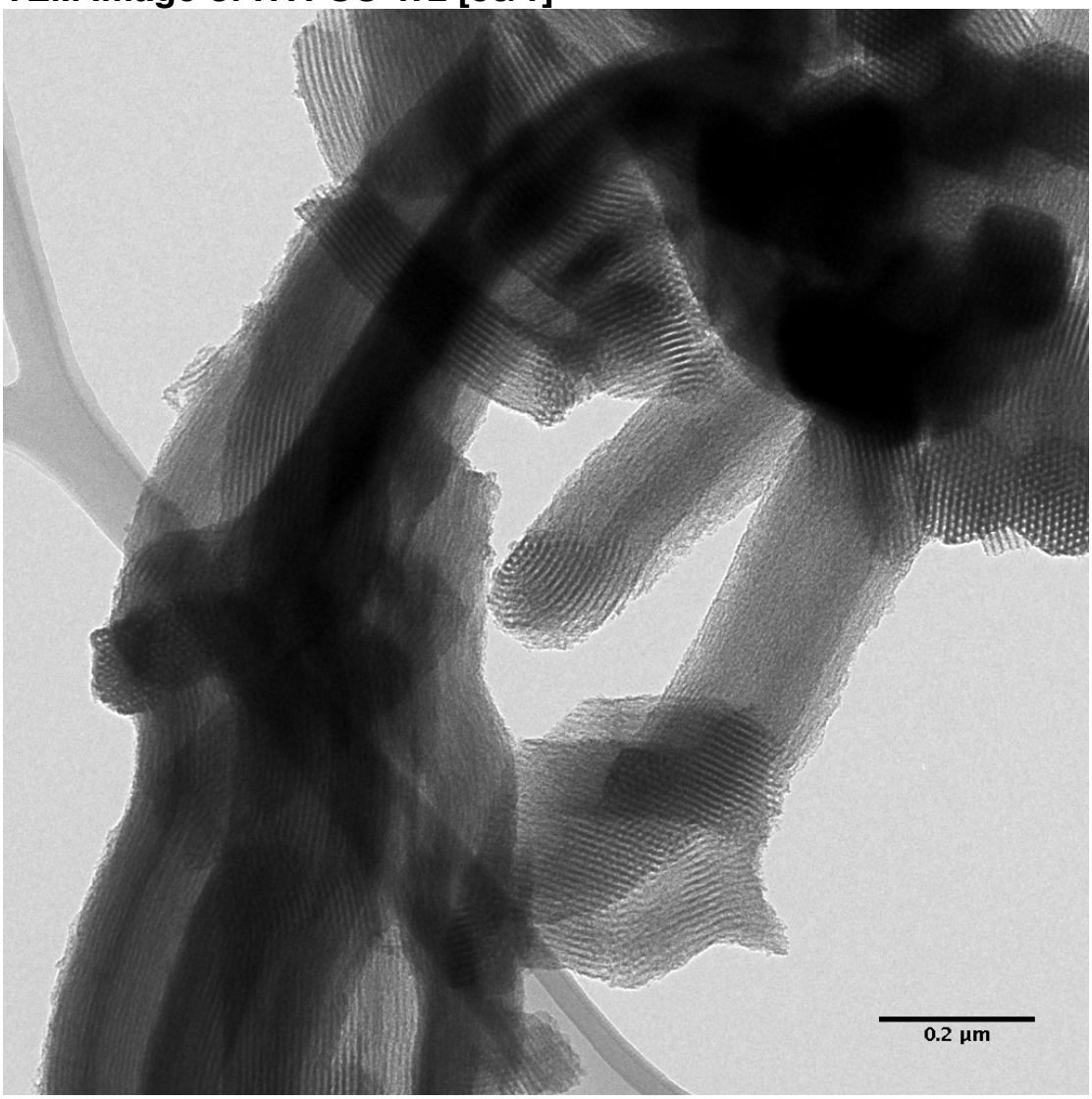

TEM Image of HYPSO-W2 [2/1]

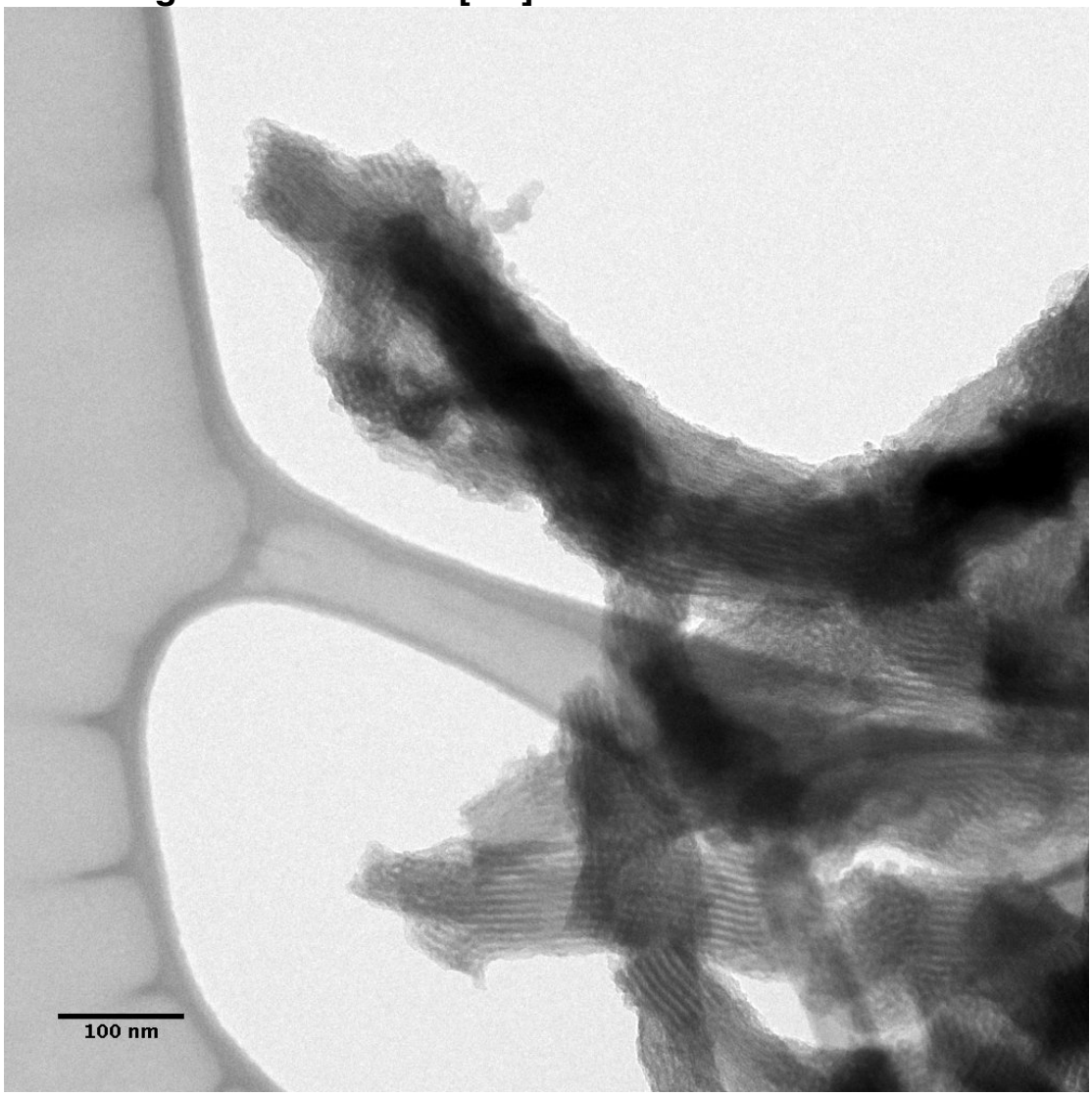

References

[1] R. G. Griffin, T. F. Prisner, *Phys Chem Chem Phys* **2010**, *12*, 5737-5740.

[2] a) A. Pines, *J. Chem. Phys.* **1972**, *56*, 1776; b) G. W. Metz, X.; Smith, S. O., *J. Magn. Reson., Ser. A* **1994**, *110*, 219–227.

[3] R. Freeman, *J. Chem. Phys.* **1971**, *54*, 3367.

[4] M. Lelli, D. Gajan, A. Lesage, M. A. Caporini, V. Vitzthum, P. Miéville, F. Héroguel, F. Rascón, A. Roussey, C. Thieuleux, M. Boualleg, L. Veyre, G. Bodenhausen, C. Coperet, L. Emsley, *J. Am. Chem. Soc.* **2011**, *133*, 2104–2107.

[5] L. Piveteau, T.-C. Ong, A. J. Rossini, L. Emsley, C. Copéret, M. V. Kovalenko, *J. Am. Chem. Soc.* **2015**, *137*, 13964–13971.

[6] M. Lelli, D. Gajan, A. Lesage, M. A. Caporini, V. Vitzthum, P. Miéville, F. Héroguel, F. Rascón, A. Roussey, C. Thieuleux, M. Boualleg, L. Veyre, G. Bodenhausen, C. Copéret, L. Emsley, *J. Am. Chem. Soc.* **2011**, *133*, 2104–2107.

[7] D. J. Kubicki, A. J. Rossini, A. Purea, A. Zagdoun, O. Ouari, P. Tordo, F. Engelke, A. Lesage, L. Emsley, *J. Am. Chem. Soc.* **2014**, *136*, 15711–15718.

[8] K. Sakai, K.-i. Yamada, T. Yamasaki, Y. Kinoshita, F. Mito, H. Utsumi, *Tetrahedron* **2010**, *66*, 2311–2315.

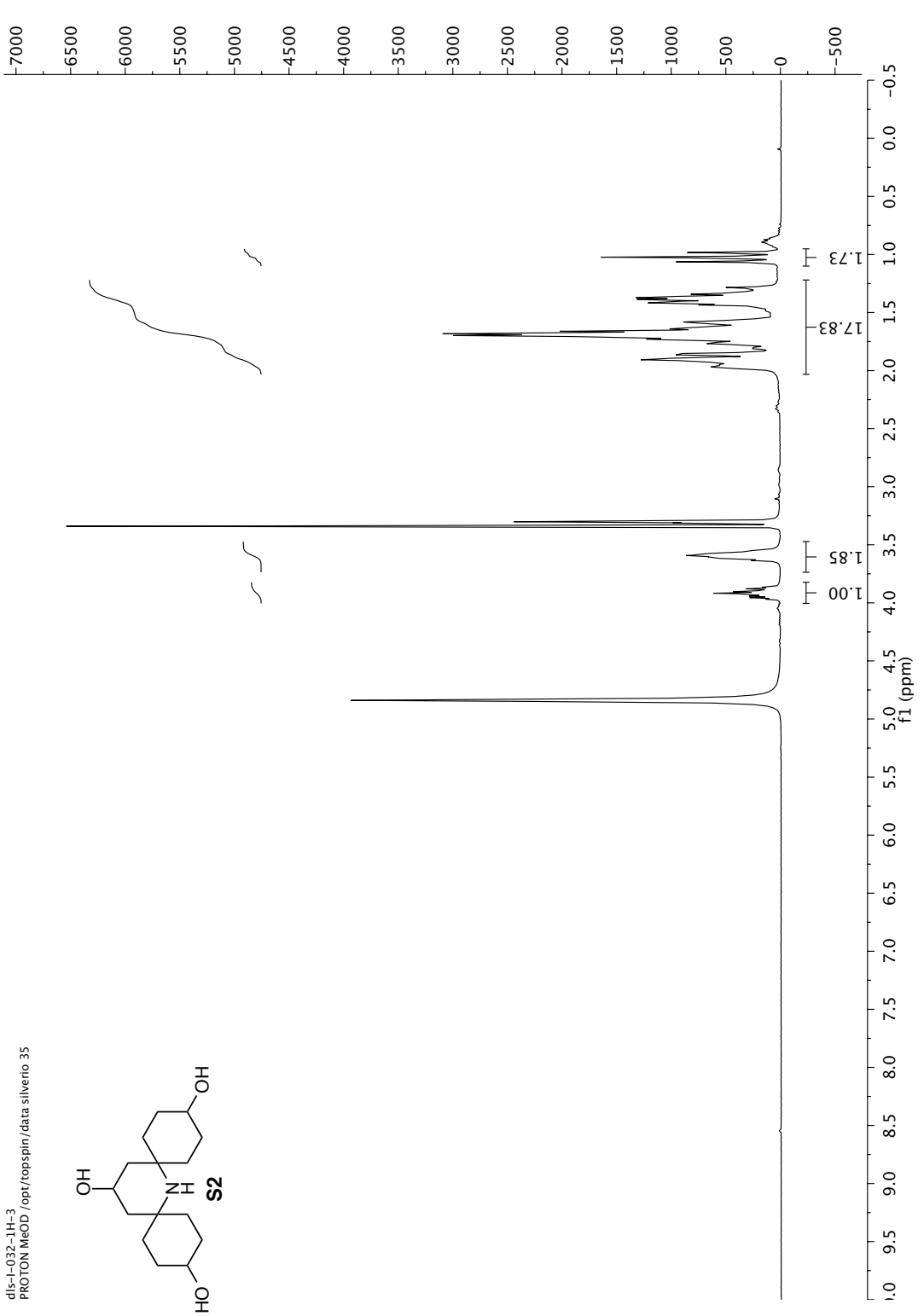
dls-I-032-1H-3
PROTON MeOD /opt/topspin/data silverio 35
OH
HO
N
H
S2
OH
1.73
17.83
1.85
1.00
f1 (ppm)

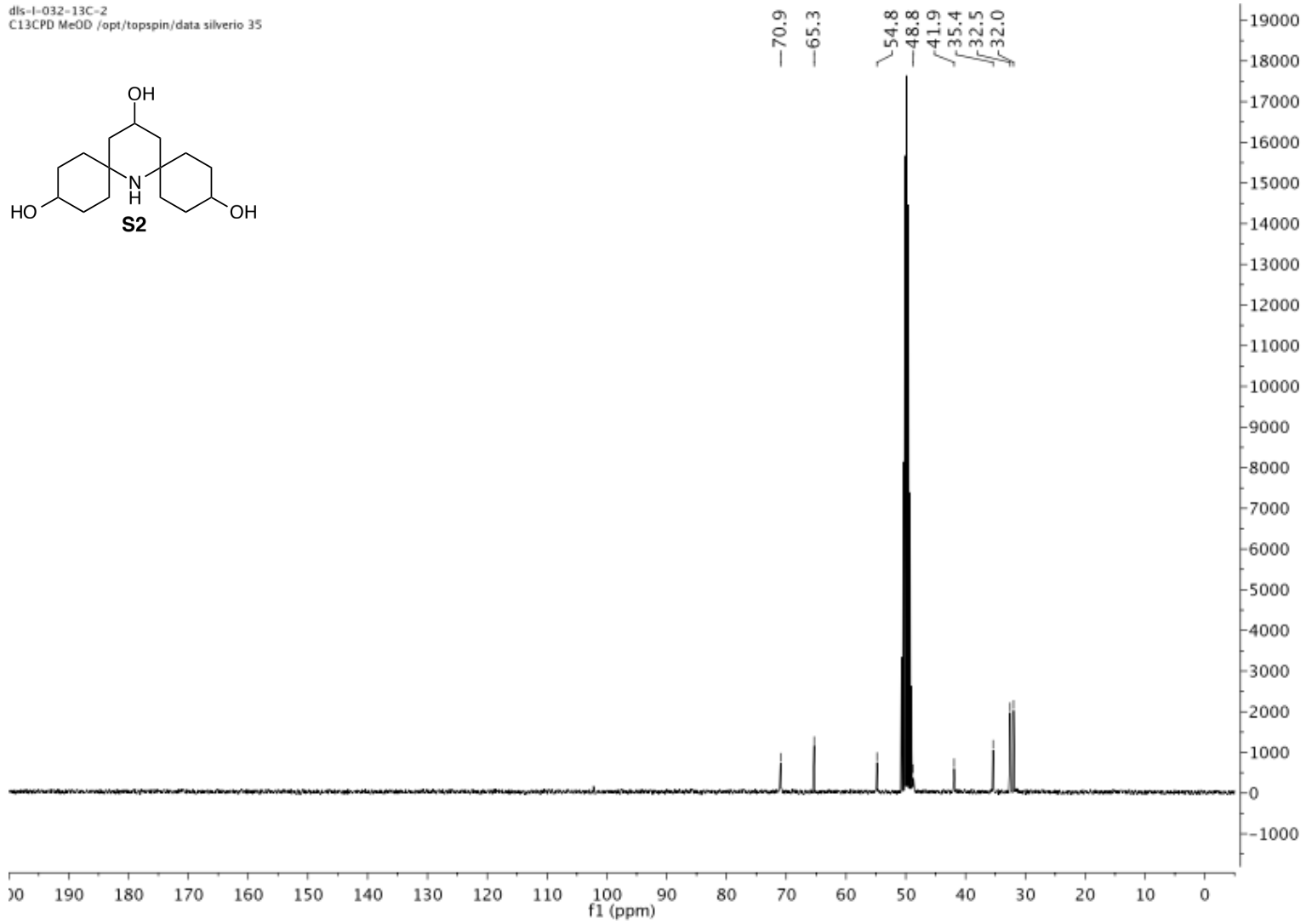
dls-I-032-13C-2
C13CPD MeOD /opt/topspin/data silverio 35
OH
N
H
HO
OH
S2
70.9
65.3
54.8
48.8
41.9
35.4
32.5
32.0
f1 (ppm)